Postfire Snow Albedo and Forest Structure Recovery Drive Decadal Watershed Scale Reductions in Snow-Water Storage and Snow Retention

A. Surunis[1] and K.E. Gleason[2]

[1] Department of Environmental Science and Management, Portland State University, Portland, OR 97201; asurunis@pdx.edu.

[2] Department of Environmental Science and Management, Portland State University, Portland, OR 97201; k.gleason@pdx.edu.

Corresponding author: Anton Surunis (a.surunis@pdx.edu)

Key Points:

- Forest fire effects on snow hydrology parameterizations enabled basin-scale estimates of postfire shifts in snow water storage and melt.
- Darkened snowpack and forest degradation decreased peak snow water storage by 4.5% and snow retention by >8 days for 15 years postfire.
- Downstream snow-water resource availability is reduced in burned forested montane watersheds across the western US for decades after fire.

Keywords: forest fire; snow water equivalent; snowmelt; snowmodel; modeling; forest structure; western US; snow; snow albedo decay; snow albedo recovery

Abstract

Forest fires darken snow albedo and degrade forest structure altering snowpack energy balance, peak snow volume and snowmelt timing for up to 15 years following burn. To date, three-dimensional volumetric estimates of postfire effects on snow hydrology over the course of postfire recovery have not been quantified at the watershed scale. Here we present an improved parameterization of recovery of forest fire effects on snow hydrology. Using a spatially-distributed snow mass and energy balance model called SnowModel, we estimate volumetric shifts in snow-water storage and snowmelt timing across a chrono-sequence of eight burned forests occurring between 2000 and 2019. One to three years following fire, postfire effects reduced peak snow-water storage by 8.42% on average (sd = 9.38%) and advanced snow disappearance date by 34 days on average (sd = 7 days). Magnitudes of snow disappearance date advances tended to decline over recovery relative to the losses observed immediately following fire. Postfire reductions in peak snow-water equivalent (SWE) tended to decrease immediately following fire, and generally recovered over 15 years postfire, but then increased again 4 to 9 years later. Postfire reductions on peak SWE summed over the 15-year postfire recovery period were up to eighteen times greater than the losses incurred in the first winter following fire alone. Beyond 15 years following fire, postfire effects on snow persisted due to the postfire shift from forest to open meadow.

Plain Language Summary

Forest fires in snowy regions burn away the forest canopy and drop burned woody debris onto the snow below. The degradation of forest cover allows more sunlight to reach the snowpack and the introduction of black carbon and burned woody debris onto snowpack darkens snow causing it to absorb more sunlight energy. These two processes cause snow to melt earlier and disappear sooner for up to 15 years following fire. We improved the ability of a snow-water model to simulate immediate postfire effects on snow and the recovery of these effects over 15 years following fire. We then quantified forest fire effects on snow volume and snow disappearance date across eight forest fires occurring over a 20-year period in the Triple Divide region of western Wyoming. We found that, in the winter immediately following fire, snow volume decreased and snow disappeared 4-5 weeks sooner. When we summed postfire effects on snow we found that postfire effects caused a 4.5% reduction in total snowpack over 15 years following fire. Earlier snowmelt drives earlier peak streamflow, earlier drying of soils in spring, and leaves surrounding forests drier for longer periods of time thereby increasing the likelihood of summertime drought and future wildfire.

1 Introduction

The American West stores approximately 50-70% of its water in snowpack with flora, fauna, and human populations relying on the slow and steady melting of this snow as a source of water in the drier periods of late spring and summer (Li et al., 2017). Warming due to climate change has reduced snow-water storage threatening annual water supply to downstream areas (Luce et al., 2013; Mote et al., 2018; Wieder et al., 2022). Due to declining snowpacks, it is predicted that spring surface water inputs will occur earlier and, without the buffering capacity provided by snow, will occur less reliably and more episodically (Barnett et al., 2005; Hale et al., 2022; Wieder et al., 2022).

Forest fires in the western United States occur predominately in the densely forested seasonal snow zone where as much as 50% of western snow falls (Gleason et al., 2013). The frequency,

severity, and extent of forest fire in the West has been increasing due to rising air temperatures and subsequent effects on seasonal snowpack and summertime soil moisture (Westerling, 2016). Forest fire in the seasonal snow zone modifies forest structure and introduces black carbon onto snow, altering the snowpack energy balance and snow ablation (Gleason et al., 2019). Canopy removal by wildfire reduces shading, subjecting greater surface areas of snow to increased solar shortwave radiative inputs and increasing wind-driven sublimation losses (Ueyama et al., 2014). Canopy removal also reduces longwave radiative inputs from vegetation, but in continental snowpack these reductions can often be counteracted by the additional inputs of solar radiative forcing due to reduced shading and increased wind ablative losses (Lundquist et al., 2013; Musselman et al., 2008; Varhola et al., 2010). In continental regions, where temperatures are colder and longwave radiative inputs from vegetation are reduced, additional solar radiative inputs from reductions in shading tend to outweigh the losses in longwave radiative inputs from forest structure degradation and result in a net increase in shortwave radiative forcing on snowpack (Lundquist et al., 2013; Musselman et al., 2008; Varhola et al., 2010). Forest fire deposition of black carbon and burned woody debris onto snowpack darkens snow albedo, enhancing shortwave radiative forcing on snowpack from the more open postfire forest structure, the rate of snow metamorphism and, subsequently, the rate of snow albedo decay following fresh snowfall (Gleason et al., 2013, 2019; Gleason & Nolin, 2016). Together, forest fires impact snow hydrology through direct and indirect reductions in snow albedo and forest structure degradation, resulting in increased postfire radiative forcing on snow, altered snowpack energy balance, decreased peak snow water equivalent (SWE), and earlier snow disappearance date (SDD) for at least 10-15 years following fire (Gersh et al., 2022; Gleason et al., 2019; Smoot & Gleason, 2021; Stevens, 2017).

The difficulty in quantifying postfire impacts on snow over large temporal and spatial scales using in-situ measurements make remotely sensed measurements a valuable tool in monitoring snow properties in remote regions over broad spatial scales. Gersh et al. (2022) utilized remote sensing derived estimates of landscape snow albedo from the National Aeronautics and Space Administration's (NASA) Moderate Resolution Imaging Spectroradiometer (MODIS) instrument's landscape snow albedo product (MOD10A1) to analyze trends in the long-term recovery of snow albedo following forest fire in the Triple Divide Region of Wyoming (Gersh et al., 2022). Results showed that landscape snow albedo steadily recovered back to an unburned open meadow state over the course of 15 years, with much of the recovery occurring in the first 10 years following the initial burn (Gersh et al., 2022). However, assessment of fine-scale snow albedo trends using MODIS data are limited by coarse resolutions and the presence of obstructions such as clouds or canopy. MODIS-MOD10A1 data are provided at a coarse spatial resolution of 500m and are not able to measure snow albedo values through clouds or other obstructions such as canopy cover (Armitage et al., 2013; Hall & Riggs, 2007; Riggs et al., 2017). Measurements of snow albedo can be influenced by fine scale landcover variability resulting in mixed pixels that do not accurately represent the albedo in a given grid cell (e.g., patchy snow cover can artificially reduce albedo measurements) (Campagnolo et al., 2016; Cescatti et al., 2012) and variability in cloud cover can result in long periods where little to no data can be retrieved from a particular study region (Armitage et al., 2013; Hall & Riggs, 2007; Riggs et al., 2017). The limited spatial extent of in-situ measurements and coarse resolution of remotely sensed measurements make process-based snow evolution models that incorporate such data an important tool in quantifying the long-term effects of forest fire on snow at a watershed scale.

To quantify the watershed-scale forest fire effects on snow-water storage and snowmelt, we used a spatially-distributed snow evolution model called SnowModel. SnowModel is a process-based model that uses first-order physics to simulate snow accumulation; blowing-snow redistribution and sublimation; snow-density evolution; and snowpack melt over spatially varying topography and landcover grids driven by temporally varying meteorological forcing fields (Liston et al., 2007; Liston & Elder, 2006a, 2006b). SnowModel was used in this study because of its basis in first-order physics, ready customizability, and extensive validation in forested, montane seasonal snowpack similar to our study region (Hiemstra et al., 2006; Liston et al., 2007, 2008; Liston & Elder, 2006a, 2006b; Sexstone et al., 2018). SnowModel utilizes four sub-models in a hierarchal modeling structure: MicroMet, EnBal, SnowPack-ML, and SnowTran-3D. MicroMet spatially interpolates meteorological forcing data from met stations observations and/or modeled reanalysis met outputs of air temperature, precipitation, wind speed, wind direction, air pressure, and relative humidity (Liston & Elder, 2006a). Using a spatially weighted Barne's interpolation method, MicroMet produces a meteorological forcing field for every cell in the simulation for every time step (Liston & Elder, 2006b). MicroMet also estimates incoming shortwave and longwave radiation inputs in each cell using solar calculations based on the latitude of the study region and parametrizations of cloudiness (Liston & Elder, 2006a). EnBal utilizes the outputs of MicroMet and physics-based mass energy balance equations to calculate the snow mass and energy balance of the snowpack within every cell at every time step of the simulation and, critical to our application, is where modeling of forest-snow interactions are handled (Liston & Hall, 1995). SnowTran-3D is a three-dimensional model that incorporates the wind-flowing forcing field from MicroMet and topographical and vegetation inputs to compute redistribution of snow due to wind and loss of snow by saltation and wind-induced sublimation (Liston et al., 2007). SnowPack-ML computes snow-density through temperature- and compaction-based snow-density evolution (Liston & Elder, 2006b). SnowPack-ML can be run using a single layer or up to 12 distinct layers and simulates cold content, permeability, and liquid water release from the snowpack within each cell for every time step (Liston & Elder, 2006b).

To date, research has shown that forest fires in the seasonal snow zone alter snow-water storage and snowmelt for at least 10-15 winters following ignition (Gleason et al., 2013, 2019; Smoot & Gleason, 2021). However, these studies have focused on point based or broad scale estimations, and no studies have quantified the watershed-scale postfire effects on snow hydrology at a fine spatial resolution and over the decades-long postfire recovery period using a physically based snow evolution model. Here, we modeled and quantified postfire impacts on snow-water storage and snowmelt metrics, including peak SWE, total snow volume, and SDD, over a chronosequence of eight forest fires occurring in the Triple Divide region of northwestern Wyoming. by incorporating a postfire effect on snow albedo and forest structure and recovery parameterization into SnowModel.

Our postfire effect on snow albedo decay and forest structure and recovery model utilized a parameterization of postfire effects on snow albedo and snow albedo decay from Gleason and Nolin (2016) and a postfire forest structure degradation and snow albedo recovery model informed by long-term trends in MODIS-derived landscape snow albedo (LSA) from Gersh et al. (2022). The parameterization of postfire effects on snow albedo and snow albedo decay was drawn from a study by Gleason and Nolin (2016) which derived empirical snow albedo decay functions from broadband snow albedo measurements taken in adjacent burned and unburned forested sites in the Shadow Lake burn region (ignition date: 2011) in the Oregon Cascades up to 3 years following fire. The parameterizations from this study characterized snow albedo decay as

an exponential function of days since snowfall for both burned and unburned forested sites and for both positive net energy balance periods (accumulation) and negative net energy balance periods (ablation) respectively for a total of four snow albedo decay functions (Gleason & Nolin, 2016). The long-term (1-15 years postfire) snow albedo recovery trends were informed by Gersh et al. (2022) which characterized postfire snow albedo recovery over years since fire in a chrono-sequence of eight burns occurring in the Triple Divide region of Wyoming between 2000 and 2018, the same burns modeled in this study. The study by Gersh et al. (2022) utilized MODIS-MOD10A1 estimates of landscape snow albedo (LSA) within the eight burn regions for up to 15 years following fire and determined, through Tukey analysis, that LSA values within the burn regions shifted to LSA values similar to that of nearby open regions over the course of 15 years following fire. The findings of these two studies provided the basis for our improved postfire snow albedo decay and recovery parameterization.

By incorporating postfire effects on snow albedo and forest structure and the associated recovery into a mechanistic model, we evaluated postfire effects on snow-water storage and snowmelt immediately following fire and over the course of a 15-year recovery period both within each forest fire perimeter and at the watershed scale. Understanding and quantifying how postfire effects on snow albedo and forest structure affect snow hydrology over many years following fire is vital as snowpacks continue to warm and forest fires increase in occurrence and extent across the West. The modeling approach and findings discussed here will help to improve understanding of the broad scale and lasting implications of forest fire effects on snow-water storage and snowmelt timing in headwaters critical for spring and summertime water supply.

2 Materials and Methods

2.1 Study Region

We evaluated the recovery of postfire effects on snow albedo and forest structure, and the associated effects on snow hydrology across a chronosequence of eight forest fires in the seasonal snow zone of Western Wyoming which burned between 2000 and 2018. The study area covers the Triple Divide region of three major river basins of the western US, including the Colorado, Columbia, and Missouri Rivers, and was determined by calculating a minimum bounding rectangle around the chronosequence of the forest fire perimeters. Forest fire perimeters were defined using the Monitoring Trends in Burn Severity (MTBS) burn perimeters data (Finco et al., 2012) plus a 2 km buffer determined within ArcGIS (Figure 1). The study domain has an average elevation of 2503m (sd = 320m) with a minimum and maximum elevation of 1727m and 3596m respectively (Danielson & Gesch, 2010). Between 2000 and 2020, the average cold season (December to March) air temperature was -7.7°C (sd = 5.5 °C) and the region received an average precipitation of 3.0 mm (sd = 4.94 mm) (NOAA, 2021; Saha et al., 2011; *USDA-NRCS*, 2020; Western Regional Climate Center, 2021). The study region is largely forested, consisting of 60% forested land and 40% unforested land (35% shrub, grassland, and agricultural, 0.006% urban, and 4% bare rock) based on Copernicus Global

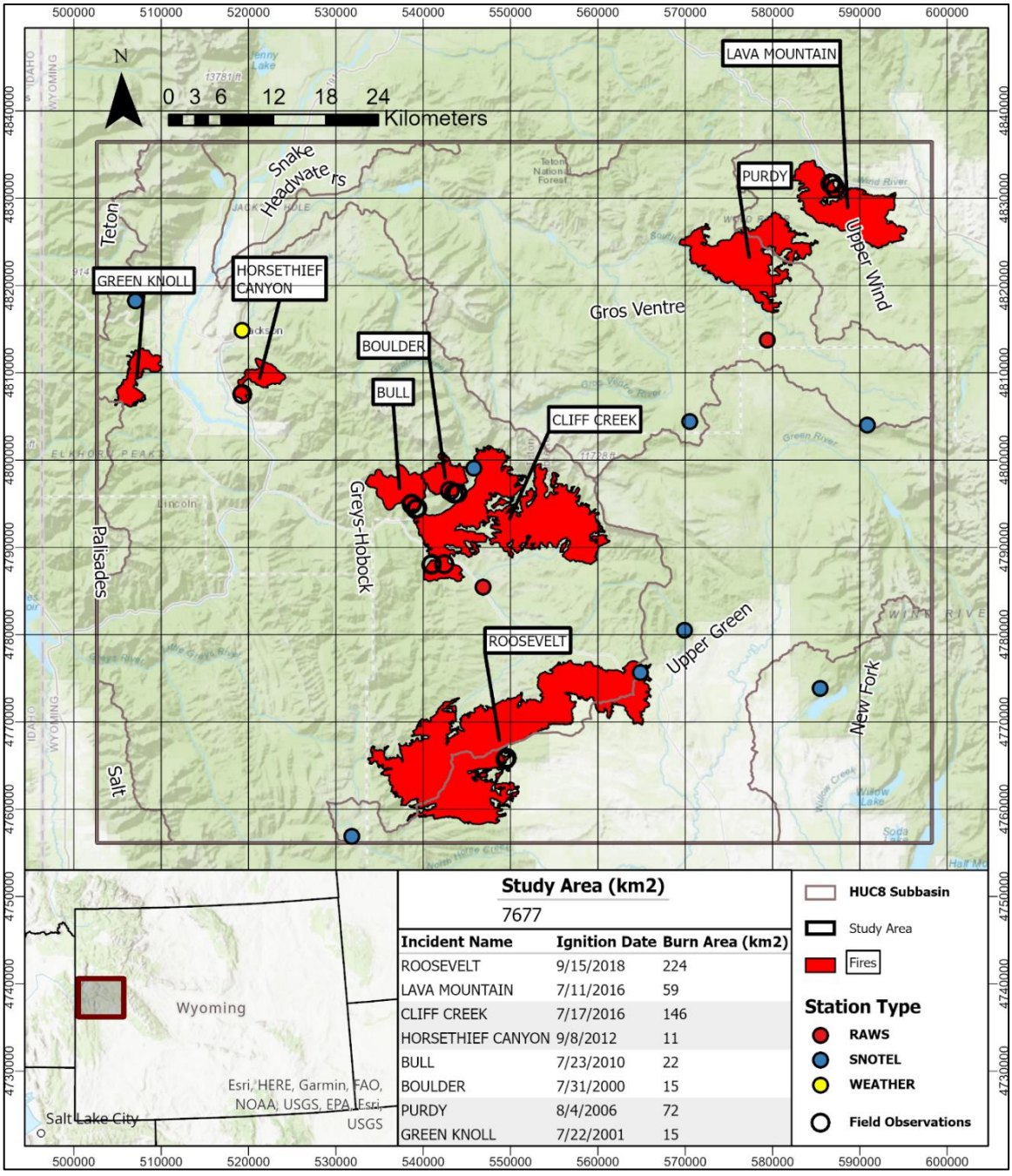

Figure 1: A map of the study region and modeling domain. The map includes Monitoring Trends in Burn Severity fire boundaries of the eight fires that occurred in the study region over the modeling time period along with their ignition date, incident type, and total burn area. The location and type of meteorological stations that the in-situ meteorological forcing data was drawn from are shown and the boundaries of the HUC-8 sub-basins and their names are also displayed.

Landcover data (Buchhorn et al., 2020). The forested land is pine-dominated, of which the most common species are Lodgepole Pine (*Pinus contorta*) and Whitebark Pine (*Pinus albicaulis*).

The study area includes the Triple Divide headwaters of three major river basins in the western US, widening the hydrological implications of forest fire effects on snow hydrology within this

196 area. Further, the study area has a history of frequent forest fire and has experienced a rapid
197 increase in the extent, severity, duration, and occurrence of forest fire in the seasonal snow zone
198 over the last decade. The combination of these two features along with the area receiving 60-
199 80% of its annual precipitation as snow (Serreze et al., 1999) makes investigation of postfire
200 effects on snow hydrology critical to preserving snow-water resources within this region and for
201 understanding postfire effects on snow throughout the West.

202 ## 2.2 SnowModel Input Data Retrieval

203 SnowModel requires three major inputs: meteorological forcing data, a topographic elevation
204 raster, and a landcover classification raster. Meteorological forcing data was retrieved from both
205 automated weather stations and modeled reanalysis data. In-situ meteorological forcing data
206 from automated weather stations were retrieved from the United States Department of
207 Agriculture (USDA) National Resources Conservation Service's (NRCS) automated Snow
208 Telemetry (SNOTEL) network (USDA-NRCS, 2020) via the National Weather and Climate
209 Center (NWCC) data retrieval tool (https://wcc.sc.egov.usda.gov/reportGenerator). SNOTEL
210 data were supplemented with additional in-situ weather data from the Western Regional Climate
211 Center's (WRCS) Remote Automated Weather Station (RAWS) network (Western Regional
212 Climate Center, 2021), and the National Oceanic and Atmospheric Administration's (NOAA)
213 Climate Data Online (CDO) network (NOAA, 2021) to capture a wider range of weather
214 variability over elevation (Table 1). Hourly measurements of air temperature, precipitation, wind
215 speed, wind direction, and relative humidity were retrieved from each of these stations and daily
216 average values of each metric were calculated for use in SnowModel. In addition, daily SWE
217 values were retrieved from the nine SNOTEL stations for SWE assimilation and later calibration
218 of SnowModel.

219 The in-situ meteorological data were supplemented with data from Climate Forecast System
220 version 2 (CFSv2) modeled reanalysis meteorological data from the NOAA National Centers for
221 Environmental Prediction (NCEP) (Saha et al., 2011). CFSv2 pixels were converted into
222 "virtual" weather stations using R's (R Core Team, 2021) "spatial" package (v7.3-12; Venables
223 & Ripley, 2002), where the coordinates of each "station" was taken as the centroid of the pixel
224 and elevation was taken as a product of geopotential height at surface. This process effectively

Table 1: List of meteorological stations used as the meteorological forcing data input or as validation data in SnowModel. Relevant metadata is provided including station type, data source, station ID number (* = validation station only), elevation in meters, easting and northing coordinates (CRS: NAD83 UTM12N), and date of the start of record.

Station Name	Type	Source	Station ID	Elevation (m)	Easting (m)	Northing (m)	Start of Record
Blind Bull Sum	SNOTEL	USDA-NRCS	353*	2637	531829	4756891	10/1/1978
East Rim Divide	SNOTEL	USDA-NRCS	460*	2417	564881	4775668	10/1/1984
Granite Creek	SNOTEL	USDA-NRCS	497*	2063	545799	4799058	10/1/1987
New Fork Lake	SNOTEL	USDA-NRCS	689*	2542	507065	4818219	10/1/1984
Gros Ventre Summit	SNOTEL	USDA-NRCS	506	2667	570509	4804425	4/1/1976
Gunsight Pass	SNOTEL	USDA-NRCS	555	2993	579829	4788969	9/1/1998
Kendall R.S.	SNOTEL	USDA-NRCS	597	2359	569894	4780482	10/1/1984
Loomis Park	SNOTEL	USDA-NRCS	661	2512	585471	4773860	10/1/1979
Phillips Bench	SNOTEL	USDA-NRCS	944	2499	590870	4803994	3/1/1976
Hoback Wyoming	RAWS	DRI-WRCS	481302	2050	546858	4785438	6/1/1996
Raspberry Wyoming	RAWS	DRI-WRCS	481307	2682	579399	4813724	6/1/1985
Jackson Airport	Weather	NOAA-CDO	USC00484910	1893	519283	4814846	1/1/1893

produced an ordered grid of weather stations across the study region. Daily values of temperature, precipitation, wind speed, and wind direction were averaged from measurements CFSv2 captures each day, and relative humidity was computed using daily averaged specific humidity value, daily average temperature, and the Clausius-Clapeyron relation (Brown, 1951).

Digital elevation maps (DEMs) and landcover classifications were retrieved using Google Earth Engine (Gorelick et al., 2017), a cloud-based and free-to-use GIS software**.** A DEM of the region was retrieved from the Global Multi-resolution Terrain Elevation Dataset (GMTED) 2010 (Danielson & Gesch, 2010). GMTED is a product of NASAs Shuttle Radar Topography Mission (SRTM), which generated a digital elevation model of elevation data at a resolution of 1 arc-second. Landcover data was retrieved from the Copernicus Global Land Cover 2015-2019 dataset which classifies 23 different classes of landcover data at a 100m resolution (Buchhorn et al., 2020). Landcover data was reclassified to match the land classes recognized by SnowModel. Both raster layers were clipped to the study region, used at their native resolutions of 100m, and converted to ASCII using R's (R Core Team, 2021) "spatial" package (v7.3-12; Venables & Ripley, 2002).

2.3 SnowModel Calibration

SnowModel was calibrated by running the base model iteratively using different sets of parameters for gap fraction, snow fraction calculations, number of snowpack layers and snowpack layer width, and scalars applied to air temperature and precipitation forcing data. Following each run, modeled SWE values were compared with the time-series of observed SWE values obtained from the SNOTEL stations within the study region. For calibration purposes, four of the nine SNOTEL stations were excluded from the meteorological inputs to use as a validation-only set. Modeled values of SWE at the observation locations were extracted by locating the cell containing each SNOTEL station and the associated observed SWE measured by the SNOTEL station for that time step. Modeled SWE depth (SWED) was then compared to the observed SNOTEL measurements using root-squared error, normalized squared error, R-squared, and percent bias (Moriasi et al., 2007). Pixel values were extracted using the "spatial" package (v7.3-12; Venables & Ripley, 2002) within R (R Core Team, 2021) and the performance statistics were calculated using the "HydroGOF" package (v0.4-0; Mauricio Zambrano-Bigiarini, 2020). Following 21 calibration runs, ideal parameters were found that met the performance thresholds outlined by Moraisi et al (2007) (Table 2). The best calibration was found using the default parameters of SnowModel, but with the modeled precipitation inputs increased by 18.5%, an amount consistent with previous research from Yuan et al (2011) that found that CFSv2 modeled reanalysis data can underestimate precipitation results by up to 20%. After calibration, SnowModel overestimated SWE by 11.40% across all stations, a level of overestimation acceptable given the performance thresholds determined by Moriasi et al (2007) ($|PBIAS| < 15\%$) (Table 2).

2.4 Model Descriptions

To quantify spatially and temporally distributed forest fire effects on snow hydrology, we used the improved postfire recovery of snow albedo and forest structure modeled over a chronosequence of burned forests in the Triple Divide region of western Wyoming. We developed three models to quantify how postfire effects on snow albedo, snow albedo decay, and

Table 2: Table showing the final performance statistics of SnowModel following pre-parameterization calibrations. The four statistics (described in the Preliminary Results section) are shown for each of the nine SNOTEL stations within the study region and the overall performance statistics are shown on the last row. The performance thresholds used for this study are also shown for each of the four statistics.

Station Name	Station ID	Elevation (m)	Easting (m)	Northing (m)	Start of Record	RSR (<0.70)	NSE (>0.50)	R^2 (>0.60)	PBIAS (|x|<15%)
Blind Bull Sum	353*	2637	531829	4756891	10/1/1978	0.34	0.89	0.90	5.10
East Rim Divide	460*	2417	564881	4775668	10/1/1984	1.03	-0.06	0.81	60.80
Granite Creek	497*	2063	545799	4799058	10/1/1987	0.29	0.91	0.93	-6.10
New Fork Lake	689*	2542	507065	4818219	10/1/1984	0.57	0.68	0.77	11.80
Gros Ventre Summit	506	2667	570509	4804425	4/1/1976	0.68	0.54	0.87	28.50
Gunsight Pass	555	2993	579829	4788969	9/1/1998	0.31	0.90	0.95	-14.60
Kendall R.S.	597	2359	569894	4780482	10/1/1984	0.28	0.92	0.92	2.20
Loomis Park	661	2512	585471	4773860	10/1/1979	0.34	0.89	0.93	10.20
Phillips Bench	944	2499	590870	4803994	3/1/1976	0.49	0.76	0.90	23.10
Overall						0.44	0.81	0.85	11.40

forest structure degradations alter snow volume and snowmelt timing over the decades-long postfire recovery period. These models included a base model, an improved postfire snow albedo recovery model, and a combined postfire snow albedo and forest structure recovery model.

2.4.1 Base model

The base model used the default, calibrated SnowModel parameters to compare against the results of the postfire forest structure and postfire snow albedo recovery models, but supplemented with the unburned forest snow albedo decay parameterizations from Gleason & Nolin (2016). The based model snow albedo decay parameterization applied time-varying exponential decay of snow albedo over days since snowfall differentially to unburned forests and open meadows during snow accumulation and snow melt periods. The base model included a snow albedo decay function but represented a simulation of the study region for 20 years with no postfire effects incorporated.

2.4.2 Postfire forest structure model

The postfire forest structure model consisted of the base model with the addition of time-varying postfire forest structure degradation parameterizations that simulated the degradation of forest structure over 15 years following fire towards that of an open meadow (Equation 3 below), but with no postfire effects on snow albedo or snow albedo decay included. The postfire forest structure model allowed for compartmentalization of postfire effects on snow hydrology due to forest structure changes versus postfire effects on snow hydrology due to postfire effects on snow albedo and snow albedo decay. The postfire forest structure model simulated only the postfire effects of forest structure degradation over 15 years without postfire effects on snow albedo.

2.4.3 Postfire snow albedo recovery model

The postfire snow albedo recovery model consisted of both an improved version of the time-decay of snow albedo parameterizations from Gleason & Nolin (2016) (Equations 1 and 2 below) as well as the forest structure degradation parameterizations from the postfire forest structure model (Equation 3). In short, this model simulated the postfire effects on snow albedo,

295 snow albedo decay, and forest structure and recovered these parameters to that of an open
296 meadow over the course of 15 years following fire.

297 2.4.4 Parameterizations of postfire recovery of snow albedo and forest structure

298 Five sets of snow albedo minima and maxima, snow albedo decay functions, and forest structure
299 parameters were computed by calculating five equally spaced values between those of an
300 immediate postburn forest and an unburned open meadow. Snow albedo minimum and
301 maximum and snow albedo decay curves for both a burned forest and an unburned open meadow
302 were drawn from Gleason & Nolin (2016), while forest structure was parameterized using
303 SnowModel's snow-holding depth values for scattered conifer forests and open meadows as the
304 immediate postfire state and post-recovery state, respectively. The snow-holding depth is used in
305 SnowModel to calculate the snow holding capacity of vegetation within each grid cell. The snow
306 depth of a cell must exceed this value before snow can reach the ground and become available
307 for wind redistribution and be subjected to wind ablation effects and canopy-modified solar
308 forcing. In order to represent the postfire snow albedo recovery, our parameterization includes
309 five recovery stages each representing 3 years of recovery in five unique snow albedo recovery
310 stages over the 15 year postfire recovery period (Figure 2). The 3-year recovery stages postfire
311 snow albedo functions and forest structure parameters were applied to each burned forest by
312 assigning custom burned forest classes using spatially distributed annual landcover rasters.

313 The improved postfire snow albedo and forest structure recovery parameterization solves for
314 daily mean snow albedo using a time-varying exponential decay coefficient, where the minimum
315 and maximum snow albedo values, and the degree of decay are modified to recover over fifteen
316 years by the five recovery periods following forest fire. The parameterization resets snow albedo
317 values following a fresh snowfall event (>5cm), and then exponentially decays over days
318 following snowfall using recovery stage specific coefficients. Maximum snow albedo ($\alpha_{snow,max}$)
319 represents the snow albedo of fresh snowfall in a burned forest as calculated by Gleason & Nolin
320 (2016). Maximum snow albedo postfire recovery rate ($\Delta\alpha_{snow,max}$) is defined as the difference
321 between $\alpha_{snow,max}$ and the snow albedo of fresh snowfall in an unburned open meadow divided by
322 five (the number of three-year recovery periods in 15 years of postfire recovery). The fresh
323 snowfall recovery rate is scaled by the number of 3-year recovery periods since forest fire (p)
324 and added to $\alpha_{snow,max}$ to produce the snow albedo of fresh snowfall in a recovering forest fire
325 (Equation 1).

326 $$\alpha_{snow} = \alpha_{snow,max} + \left(p * \Delta\alpha_{snow,max}\right) \quad (1)$$

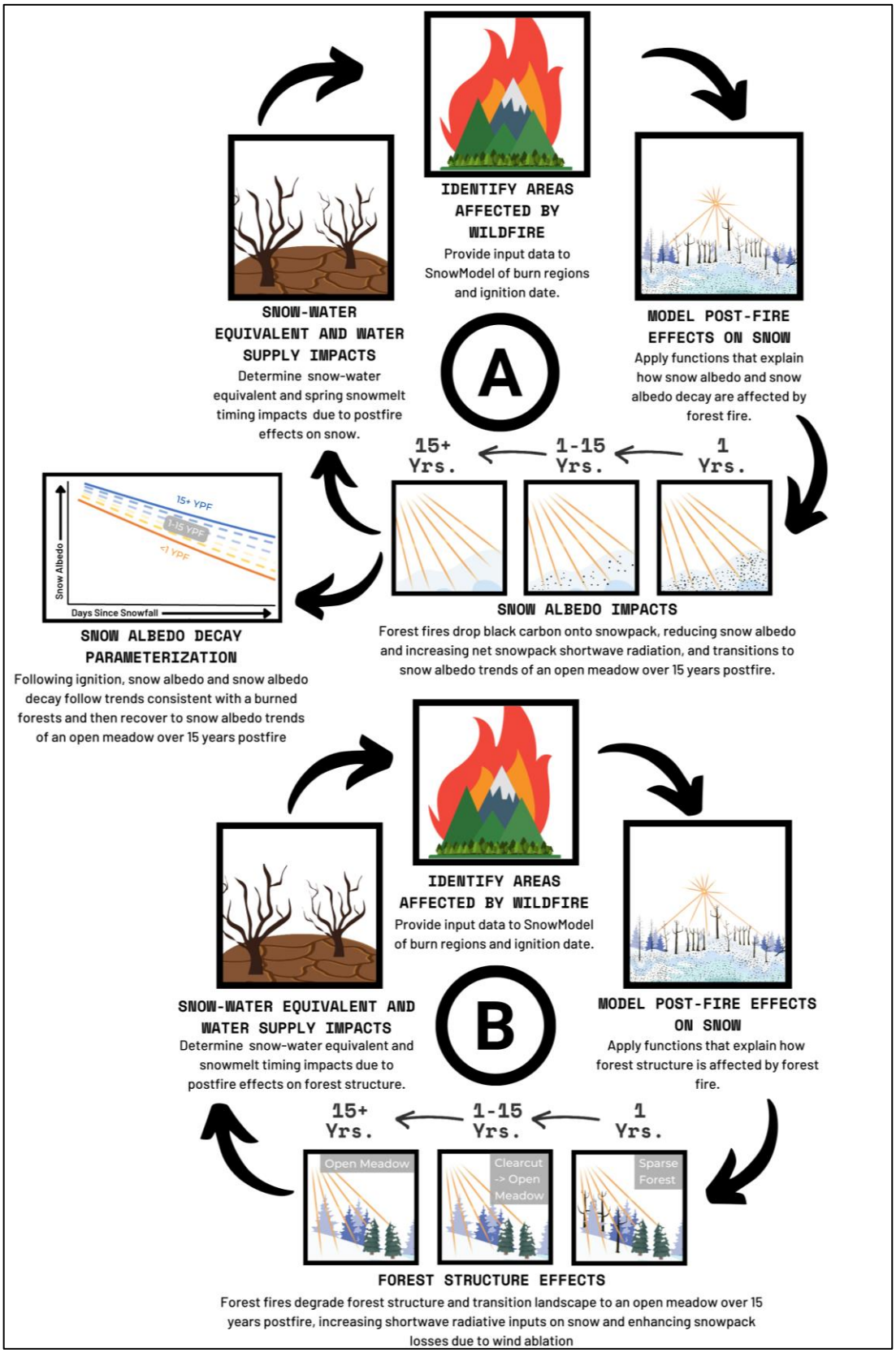

Figure 2: A conceptual model of the postfire snow albedo recovery (A) and postfire forest recovery (B) models.

327 Unburned forests exponentially-decay as a function of daily time steps per the calculations

defined in Gleason & Nolin (2016). In burned forests, snow albedo decayed using an exponential decay coefficient that was adjusted to account for postfire recovery periods over 15 years following forest fire (Equation 2). Snow albedo in days following fresh snowfall ($\alpha_{snow}{}^{n+1}$) is calculated in the same way as Gleason & Nolin (2016) and Equation 1 except the minimum snow albedo of a burned forest ($\alpha_{snow,min}$) and the exponential snow albedo decay rate (K_a) are adjusted by the minimum snow albedo recovery rate ($\Delta\alpha_{snow,min}$) and the snow albedo decay recovery rate (ΔK_a), respectively, with each rate scaled by the current recovery period (p).

$$(\alpha_{snow})^{n+1} = (\alpha_{snow,min} + \Delta\alpha_{snow,min} * p) + \left((\alpha_{snow})^{n} - (\alpha_{snow,min} + \Delta\alpha_{snow,min} * p\right)^{[(-K_\alpha + \Delta K_\alpha * p) * dt]} \quad (2)$$

To represent the postfire "recovery" of landcover change from burned forest to an open meadow following fire, the burned forest class snow-holding depths were adjusted by the landcover recovery rate (ΔSHD) from a scattered conifer forest to a sparse open meadow scaled by the postfire recovery period (p) using the default values for the endmembers of those landcover classes included in SnowModel (Equation 3).

$$SHD_{burn} = SHD_{forest} - (\Delta SHD * p) \quad (3)$$

2.5 Analysis of Model Results

2.5.1 Postfire effects on snow-water storage and snow disappearance date

Postfire effects on snow hydrology was evaluated by differencing results from the base model from the results of the postfire snow albedo and forest structure recovery models. Spatially and temporally integrated forest fire effects on snow-water storage were evaluated by differencing peak SWE raster for each year in the 20 year modeling period. Peak SWE rasters were created by determining the maximum SWE for each grid cell for each water year, and differenced from the base model minus the postfire models, then averaged for burned forest in the chronosequence for each recovery period following fire. Volumetric changes in peak SWE for each burned forest were calculated by multiplying the peak SWE differences by the spatial resolution (100 m^2), summing the volumetric differences of each grid cell within each burn region, and then averaging the total volumetric change in peak SWE.

Postfire effects on snow disappearance date (SDD) were quantified by determining the day of year of snow disappearance for each grid cell for each water year and differencing the postfire snow albedo or forest structure recovery model results from the base model results. SDD was defined as the first day following peak SWE in which a grid cell reached zero SWE depth for each year. Base model annual SDDs were then differenced from the postfire snow albedo recovery model SDDs and the SDD differences were averaged over the first year postfire, each three-year bin following fire, and 16+ years postfire according to the ignition date of each fire.

2.5.2 Postfire effects on snow hydrology over space, time, and recovery

Spatially and temporally integrated and differenced postfire effects snow hydrology metrics were evaluated monthly including, March 1st to represent accumulation, April 1st to represent the start of ablation, and May 1st to represent ablation to produce three change in SWE rasters for each

date and each year for each fire. The differenced rasters were then averaged in three-year bins for every three years following fire effectively producing a period-averaged March 1st, April 1st, and May 1st differenced raster for each three-year postfire recovery period. The average proportional change in SWE and 95% confidence interval were also calculated for each raster. Daily SWE depth plots were created for each burn over the recovery period to highlight differences in how snow accumulates and melts in forests affected by forest fire over recovery. For each burn, SWE depth values in each pixel were averaged for each daily time-step for all three models. These values were then averaged over period to produce period-averaged SWE for each day of the water year for each recovery period. All calculations were computed using base R (R Core Team, 2021) and the "spatial" package (v7.3-12; Venables & Ripley, 2002). These analyses were performed on all modeled forest fires, but only the results of the Roosevelt forest fire (Ignition Date: 2018) and Green Knoll forest fire (Ignition Date: 2001) were included here as examples illustrating immediate and long-term postfire effects on snow, respectively.

2.5.3 Postfire effects on snow hydrology at the watershed scale

Watershed scale impacts of postfire effects and recovery on ablation season (May) SWE were investigated within the Lower Granite Creek Hydrologic Unit Code 12 (HUC12) subbasin. We chose to focus on the ablation season for two reasons: 1) postfire effects on snow hydrology were most pronounced following peak SWE and 2) estimations of SWE reductions due to postfire effects would likely be most applicable to watershed managers during the melt season when snowpack is melting off. A United States Geological Survey (USGS) delineation of the watershed was extracted using the Living Atlas tool in ArcGIS (Esri Inc., 2022) and exported into R (U.S. Geological Survey National Geospatial Program, 2022). Annual changes in ablation SWE due to postfire effects were quantified by calculating the average proportional and volumetric difference in SWE within the watershed between both models. Total SWE difference over 20 years between both models was calculated by summing the differences in ablation SWE and converting to volume. Corresponding annual ablation SWE depth rasters from the base model and postfire snow albedo recovery model were differenced, clipped with the watershed delineation file, and plotted using the "spatial" package (v7.3-12; Venables & Ripley, 2002) in R (R Core Team, 2021).

2.5.4 Significance testing

We tested for statistically significant differences between the base model and postfire snow albedo recovery model using the extracted values of peak SWE, SDD, seasonal SWE (March, April, and May), and watershed SWE. Differences between the base model and postfire snow albedo recovery model results were tested for statistical significance using a two-sided, two-sample Welch t-test using an alpha value of 0.05. All results were analyzed for statistical significance on a subset of paired random samples of 20% of the grid cells within each burn region from the base model and postfire snow albedo and forest structure recovery model rasters and running the t-test using base functions within *R* (R Core Team, 2021).

2.5.5 Model validation

Modeled SWE outputs from the base model and postfire snow albedo recovery model were validated using field measurements of SWE taken from six of the modeled burns (Horsethief

Canyon, Bull, Boulder, Cliff Creek, Lava Mountain, and Roosevelt) during February and March of 2019 (Figure 1). Prior to validation, the field data were preprocessed using R (R Core Team, 2021). Originally, the 114 SWE measurements were collected inside and outside the burn so we first subset the measurements based on measurements that fell within the MTBS burn boundaries of each of the six fires. At each site within the burns, one to three replicates of SWE measurements were taken and, due to the close proximity of the replicates and the modeling resolution of 100 m^2, replicates were averaged as they always fell within the same modeled pixel. Average measured values were then matched with corresponding modeled SWE results from the base model and postfire snow albedo recovery model using their geographic coordinates and date of collection and the average percentage difference between the values were computed for each fire. An an overall average percentage difference was calculated by computing average percentage difference between all observed measurements and the associated base model SWE and postfire snow albedo recovery model SWE.

3 Results

3.1. Summary

Postfire reductions in snow albedo and forest structure degradation decreased snow-water storage and advanced snow disappearance date persistently for up to 15 winters following ignition across all modeled forest fires (Table 3). Immediately following fire, snow volume increased slightly during the accumulation period (March 1st), but increased solar forcing from postfire canopy loss and postfire reductions in snow albedo drove earlier melt onset, leading to profound reductions in April and May snow volume (Figure 4). Earlier melt onset resulted in reduced peak snow water volume and earlier SDDs immediately following fire and throughout the 15-year postfire recovery period (Figure 4) with reductions in peak SWE increasing in magnitude 4 to 9 years later (Table 3). Burned forests modeled beyond postfire recovery (>15 years postfire) still showed lasting changes in peak SWE and SDD 16+ years following fire (Figure 4; Table 3). At the watershed scale, postfire effects and recovery of three burns modeled in the Lower Granite Creek sub-basin caused net reductions in May 1st SWE in all but one year, with the greatest net reductions in May 1st SWE occurring 3 to 5 years following each burn (Figure 6).

3.2. Immediate postfire effects on snow volume and snow disappearance date

In the winter immediately following fire, postfire effects decreased peak SWE (-8.42%, sd = 9.38%; $p < 0.001$) and advanced SDD by about 5 weeks (34 days, sd = 7 days; $p < 0.001$) on average across all modeled burns (Table 3). Peak SWE shifts one-year postfire varied greatly across burned forests (range of -1.43% to -23.65%) despite their close proximity to one another and identical postfire parameterizations.

The Roosevelt forest fire provides an example of postfire effects on snow in the winter immediately following fire. Changes in peak SWE and snow disappearance date in the Roosevelt forest fire were consistent with the changes observed across all modeled forest fires one to three years postfire (peak SWE = - 9.34%; $p < 0.001$) and thus the forest fire serves as a good example of both postfire effects on snow in the years immediately following fire and contemporary trends in Western forest fire regimes (Table 3). Over the two winters following the Roosevelt forest

Table 3: Calculations of the differences in volumetric SWE (Snow-Water Equivalent) (<1 year postfire, total, and per period) and differences in snow disappearance date (SDD) between the base model and postfire albedo model. Nearly all modeled fires showed average reductions in peak SWE and advances in SDD relative to the base model in every recovery period following fire. Reductions in peak SWE summed over up to 15 years of recovery were 2 to 18 times greater than the peak SWE losses occurring immediately following fire. In the two burns modeled for the entire 15-year postfire recovery period, peak SWE losses were 7 to 18 times greater than the peak SWE losses 1 year postfire. Over postfire recovery, the greatest losses in peak SWE often did not occur immediately following fire, but instead 4-9 years later. The greatest shifts in SDD tended to occur immediately following fire and then decreased over 15 years following fire with slight fluctuations in this trend. Cells are colored in severity of the change for each burn, with red indicating more severe losses and blue indicating relative gains. The ignition year, total burn area, average elevation, and altitudinal variability for each burn region are included above. Asterisks are also shown on all SWE metrics denoting the level of significant difference between the base model and postfire albedo model (blank: not significantly different, *: $p < 0.05$, **: $0.001 < p < 0.01$; ***: $p < 0.001$).

Burn	Immediate Peak SWE Loss (<1 YPF)	Period 1 (1-3 YPF)	Period 2 (4-6 YPF)	Period 3 (7-9 YPF)	Period 4 (10-12 YPF)	Period 5 (13-15 YPF)	Post-Rec. (16+ YPF)	Total Peak SWE Change (1-15
Boulder	-7.87%***	-7.64%***/ 4.00%	-5.31%***/ 3.03%	-5.42%***/ 3.54%	-1.06%***/ 7.05%	-2.65%*/ 2.73%	+1.93%***/ 3.16%	-4.13%***
Green Knoll	-16.93%***	-11.93%***/ 4.05%	-14.93%***/ 4.43%	-7.10%***/ 8.28%	-6.67%**/ 3.92%	-6.05%***/ 5.46%	-2.51%***/ 4.12%	-8.09%***
Purdy	-6.28%***	-3.52%***/ 9.69%	+0.30%***/ 11.50%	-2.03%***/ 6.28%	+0.99%***/ 5.20%	+4.48%***/ 7.80%		-0.65%
Bull	-1.43%	-9.23%***/ 5.73%	-5.99%***/ 1.93%	-6.97%***/ 3.36%	-0.08%/ 6.32%			-6.26%***
Horsethief Canyon	-23.65%***	-14.85%***/ 4.73%	-10.97%*/ 5.28%	-6.30%*/ 2.79%				-10.57%***
Lava Mountain	-7.50%***	-6.14%***/ 3.73%	+5.34***/ 9.16%					-3.60%***
Cliff Creek	-9.11%***	-6.96%*/ 6.39%	-4.27***/ 11.12%					-6.12%***
Roosevelt	-9.34%***	-6.85%***/ 7.47%						-6.54%***
Avg. Peak SWE Change (%)	8.42%***/ 9.38%	-6.81%***/ 11.23%	-3.14%***/ 13.43%	-3.90%***/ 8.71%	-0.92%***/ 9.37%	+0.86%***/ 9.82%	-0.30%***/ 4.29%	-4.46%***/ 11.43%
Avg. Peak SWE Change (m^3)	-4.34M***/ 5.03M	-8.13M***/ 7.49M	-1.78M***/ 1.77M	-2.27M***/ 1.19M	-0.16M***/ 1.31M	+0.64M***/ 2.95M	-0.09M***/ 0.34M	-10.96M***/ 7.02M
Avg. SDD Shift (days)	-34 days***/ 7 days	-31 days***/ 9 days	-27 days***/ 13 days	-22 days***/ 8 days	-17 days***/ 6 days	-8 days***/ 6 days	-5 days***/ 6 days	

fire (2019 and 2020), average March 1st SWE increased (6.93 ± 1.21%, $p = 0.017$) driven primarily by the more open postfire forest canopy (Figure 3a) with postfire snow albedo reductions causing a minimal net increase in solar shortwave inputs (Figure 5a). Average April 1st SWE in the postfire snow albedo recovery model was not significantly different than in the base model, indicating that the increase in March 1st SWE observed earlier was lost, primarily due to earlier melt onset from postfire effects on snow albedo (Figure 3b and Figure 5a). Following April 1st, melt onset began in earnest in the postfire snow albedo recovery model while snow continued to accumulate until mid to late April in the base model and postfire forest structure model (Figure 3d), an indication that earlier melt onset was primarily driven by postfire effects on snow albedo. By May 1st, average snowpack volume within the Roosevelt burned forest had decreased significantly (-45.76 ± 27.41%, $p < 0.001$) in the postfire snow albedo recovery model as a result of the earlier melt onset and decreased average peak SWE (Figure 3c). Earlier melt onset and decreased average peak SWE in the Roosevelt burn then culminated in a

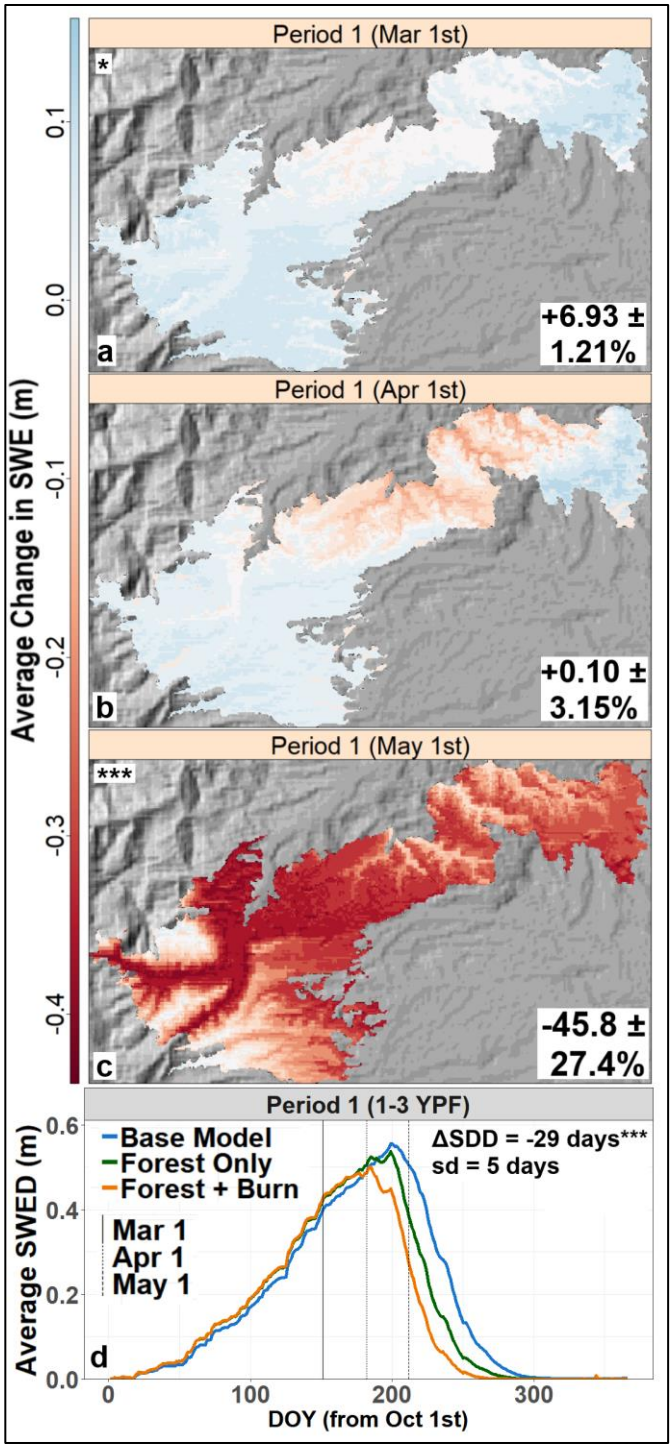

Figure 3: Change in snow-water equivalent (SWE) depth between the base model and postfire snow albedo recovery model in Roosevelt forest fire (Ignition Year: 2018). Postfire effects caused small increases in average March 1st SWE (a), no significant difference in average April 1st SWE (b), and large reductions in average May 1st SWE (c) across the burn region. Prior to April 1st, the average SWE of the postfire forest and postfire albedo model was greater than the base model (d).

29-day earlier average snow disappearance date (sd = 5 days; $p < 0.001$) over the full data record for the Roosevelt Fire of two years following fire (Table 3).

3.3. Recovery of postfire effects on snow volume and snow disappearance date

Postfire effects on snow albedo and forest structure steadily recovered over 15 years following fire, yet subsequent changes in peak SWE and SDD did not follow the same trend. Average postfire reductions in peak SWE tended to decrease in magnitude from 1 to 6 years postfire (-6.81% to -3.14%; $p < 0.001$) but increased in magnitude 4 to 9 years postfire, with this increase occurring in most fires 7 to 9 years postfire (-3.14% to -3.90%; $p < 0.001$) (Table 3). Across all burns, peak SWE reductions were also most variable in this same period (4-6 YPF: sd = 13.43%). Despite identical parameterizations across each burn and averaging over across time and climatology, changes in snow hydrology were still highly variable 4-6 years postfire and suggesting that diversity in landscape and elevation was responsible for much of the variability in postfire snow hydrology.

The Green Knoll forest fire provides an example of the long-term recovery of postfire effects on snow. In the Green Knoll forest fire, the greatest reductions in peak SWE over postfire recovery did not occur immediately following fire, but instead 4-6 years postfire (-14.93%, sd = 4.43%, $p < 0.001$) (Table 3). Over 15 years of postfire recovery, postfire effects on snow albedo and forest structure in the Green Knoll burn caused small increases and decreases in accumulation season SWE 1 to 15 years postfire (range: -1.60% ± 5.75% to +7.13% ± 12.93%, $p < 0.001$; Figure 4a). Accumulation period SWE (March 1st SWE) averaged over period was

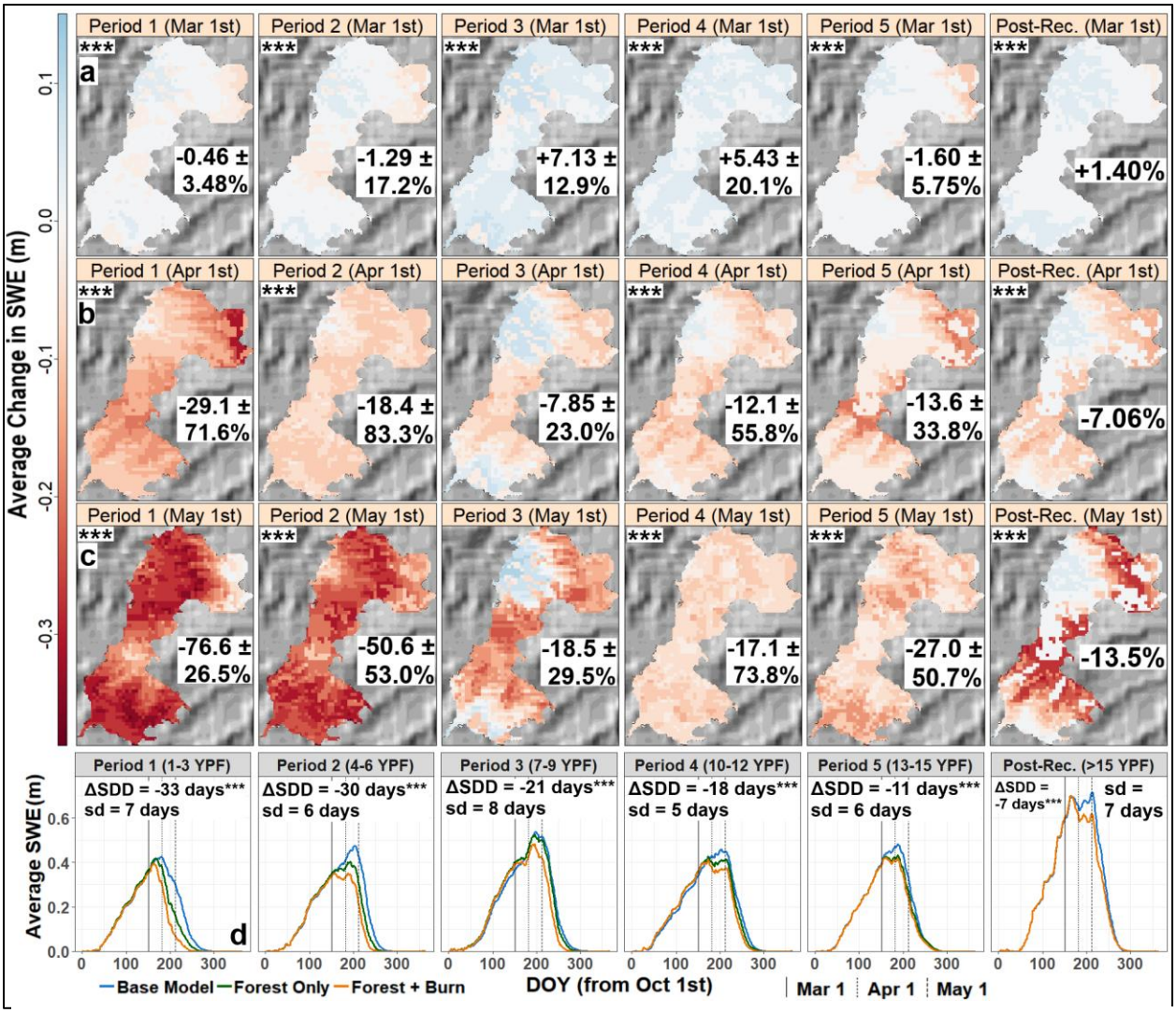

Figure 4: The change in snow-water equivalent depth (SWE) depth between the base model and postfire snow albedo recovery model in the Green Knoll fire (Ignition Year: 2001). Over 15 years of postfire recovery, postfire effects caused slight changes in SWE during March 1st (a), but then caused modest reductions in April 1st SWE (b), followed by profound reductions in May 1st (c). Postfire changes in SWE tended to reduce in magnitude over each successive recovery period, but, critically, post-recovery reductions in SWE were still present 16+ years following fire (d).

similar between the postfire snow albedo recovery model and postfire forest structure model for all recovery years, indicating that accumulation patterns over recovery were likely driven by postfire effects on forest structure and that postfire effects on snow albedo play a smaller role in affecting snow accumulation during this period (Figure 4d). Average reductions in SWE in the postfire snow albedo recovery model began to manifest during April and May of each winter 1 to 15 years following fire. Start of ablation SWE (April 1st SWE) decreased in the postfire snow albedo recovery model relative to the base model across the 16+ year recovery period (range: -29.12% ± 71.64% to -7.85% ± 23.01%) with significant reductions occurring 1-6 years postfire and 10-12 years postfire ($p < 0.001$) (Figure 4b). Snowmelt period SWE (May 1st SWE) profoundly decreased in the postfire snow albedo recovery model across the recovery period (1 to 15 years postfire) (range: -76.63% ± 26.47% to -17.05% ± 73.76%), with significant average

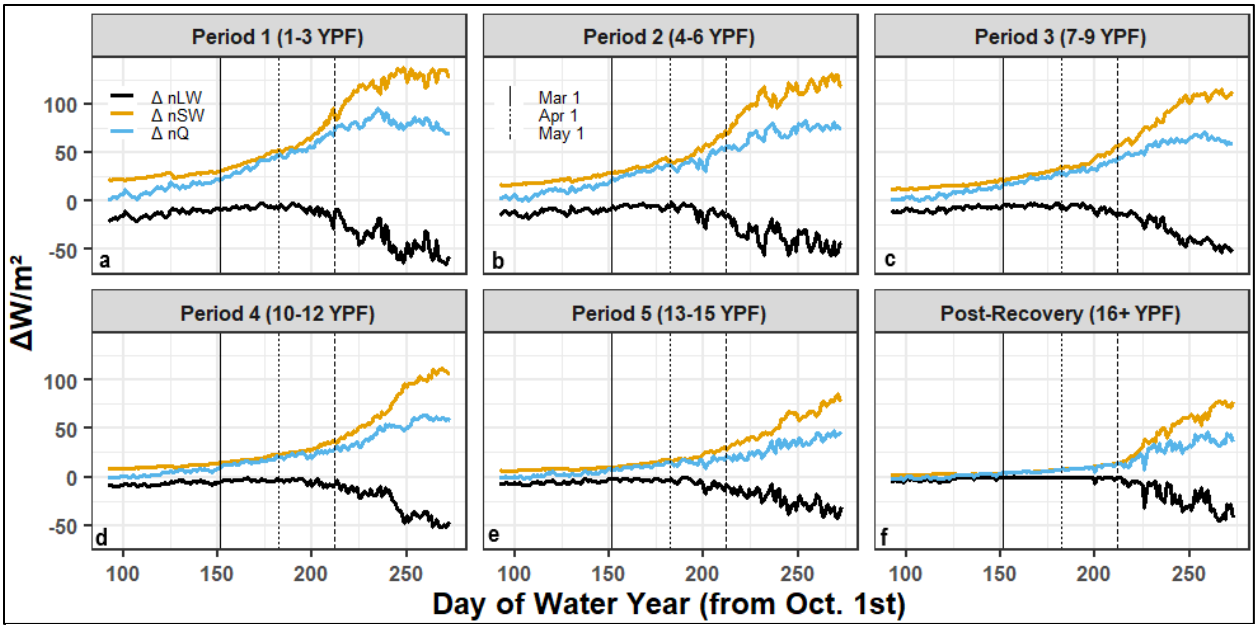

Figure 5: Difference between base model and postfire albedo model net components of the snowpack energy balance averaged over 3-year bins since burn. The progressively more open postfire canopy allowed for increased solar shortwave incident on the snow surface over years since fire, but increasing snow albedo over years since fire drive the increases in internal snowpack energy and associated changes in snowpack volume. The difference in net shortwave inputs between models decreases over years since fire showing that postfire effects on snow albedo drive changes in peak snowpack volume over 15 years postfire and beyond.

reductions occurring in all years except 7-9 years postfire ($p < 0.001$) (Figure 4c). SWE reductions present in April and May reflect the postfire shift to earlier melt onset which tended to occur prior to April 1st for all years 1-15 years postfire (Figure 4d). Average SWE in the postfire snow albedo recovery model began to diverge from the postfire forest structure model during peak SWE (April 1), (1 to 12 years postfire), with the postfire forest structure model continuing to accumulate snow beyond April 1st (Figure 4d). Alterations in the snowpack energy balance during this period were dominated by additional shortwave solar inputs (Table A2-A3; Figure 5). Additional shortwave radiative forcing due to postfire degradation of forest canopy accounted for the majority of added inputs relative to postfire effects on snow albedo (54.0-18.9% vs. 29.2-0.00%) (Figure A1-2; Figure 5).

Snow disappearance date advanced by a month immediately following fire and earlier snow disappearance persisted across all postfire recovery years (1-15 years postfire) in the postfire snow albedo-forest model, with the greatest advances in SDD occurring 1-3 years postfire (-31 days, sd = 9 days; $p < 0.001$) (Table 3). Even after 15 years following fire SDD remained 5 days earlier in the postfire snow albedo and forest recovery models than the base model, due to the postfire landcover recovering from burned forest to open meadow after 15 years following fire. Advances in SDD decreased over the 15 year postfire recovery period evaluated, with slower recovery between 1 to 12 years postfire (14 days over 12 years) and rapid recovery 12 to 15 years postfire (9 days over 3 years) (Table 3).

In total, postfire effects on peak SWE summed over 15 years of postfire recovery and averaged across all burns amounted to a total reduction in snow volume of 10.96M m^3 (sd = 7.02M m^3; $p < 0.001$) or 4.46% reduction (sd = 11.43%; $p < 0.001$), double the loss in snow volume

immediately in the 1st year postfire (4.85M m^3/8.42%; sd = 5.03 m^3/9.38%; $p < 0.001$/$p < 0.001$) (Table 3). In the post-recovery period (16+ years postfire), peak SWE still was reduced in the Green Knoll burn region (-2.51%, sd = 4.12%; $p < 0.001$) (Table 3). Post-recovery, accumulation period (March 1st) SWE increased by +1.40% ($p < 0.001$) on average (Figure 4a), while peak SWE and snowmelt period (April and May) SWE was still reduced due to the post recovery shift in snow albedo and forest parameterizations to open meadow (April: -7.60%, $p < 0.001$; May: -13.50%, $p < 0.001$) (Figure 4b-c). During this period, recovery of changes in the snowpack energy balance were primarily attributed to changes in net shortwave energy (Figure 5f; Table A3) and these changes in net shortwave energy were primarily driven by increases in outgoing shortwave (Figure A1f). Thus, the recovery of peak SWE was primarily driven by the recovery of snow albedo occurring from the transition of postfire forest to an unburned open meadow rather than due to changes in forest canopy degradation over the same transition (Figure A1f; Figure 5f).

3.4. Effects of postfire impacts and recovery at the watershed scale

Integrating forest fire effects on snow albedo and forest structure recovery across the subbasin showed long-lasting and persistent reductions in snow-water storage at the watershed scale particularly in the ablation period (May). Here, we focus on postfire effects on snow hydrology during the ablation period as 1) postfire effects on snow albedo and forest structure caused the greatest reductions in snow water storage at the watershed scale in the ablation period and 2) estimations of postfire effects on snowmelt timing and volume during ablation have greater applicability to watershed hydrology and watershed management . Three of the modeled forest fires (Boulder, Bull, and Roosevelt) occurred entirely or partially within the Lower Granite Creek (LGC) subbasin. The Boulder forest fire was the earliest occurring burn (2000) and took place entirely within the LGC subbasin (15 km^2; 13.05% of the watershed area), while the Bull and Roosevelt fires occurred partially within the LGC subbasin (burning 12 km^2 [10.48%] and 23 km^2 [19.81%] of the basin, respectively) (Figure 6). In combination, all three fires burned 43.37% of the watershed area over the 20-year modeling period (50.45 km^2) (Figure 6).

Forest fires in the LGC subbasin largely caused annual losses in ablation season snow volume over 20 years (average 6.30 ± 6.95% loss in May 1st SWE) with the greatest proportional losses in SWE occurring during 2015 and 2019 (-9.50 ± 68.0% and -14.58 ± 76.1%; $p < 0.001$) (Figure 6). During 2015, postfire effects from both the Boulder and Bull forest fires impacted snow volumes within the LGC subbasin (both burns occurred <15 years prior) and, combined, caused a 9.50 ± 68.80% reduction in May 1st SWE ($p < 0.001$). During 2019, postfire impacts from the Cliff Creek burn (occurring 3 years prior) caused a 14.58% reduction in May 1st SWE in combination with the postfire recovery effects from the Bull forest fire (occurring 9 years prior) (Figure 6; 2012 and 2019). Forest fires relatively late in their postfire recovery continued to cause losses and enhanced immediate losses from more recent burns. Repeated burns within the LGC subbasin and the associated postfire impacts on snow and forest structure resulted in a total

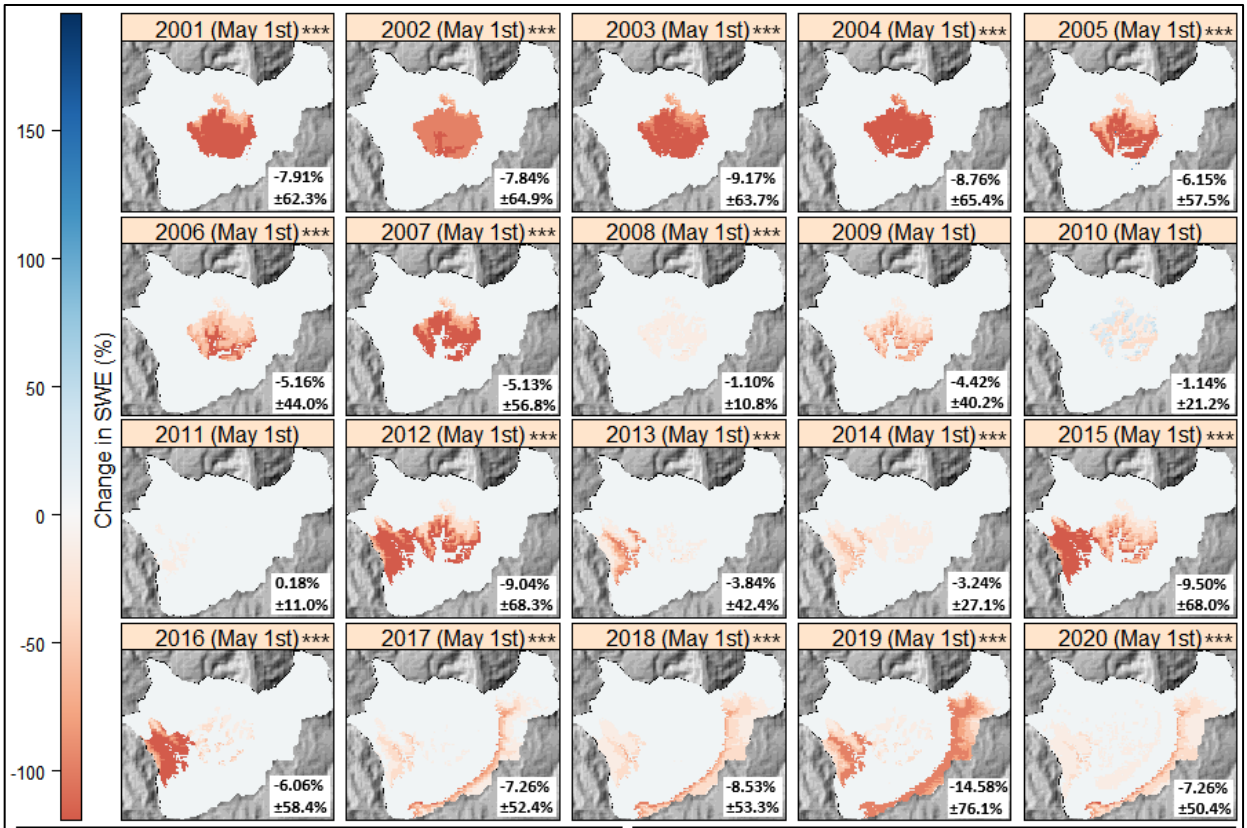

	Boulder	Bull	Cliff Creek
Ignition Year	2000	2010	2016
Watershed Area Burned (%)	13.05%	10.48%	19.81%
Watershed Area Burned (km²)	15.18	12.19	23.05

	Proportion	Absolute
Total Watershed Area Burned	43.37%	50.42 km²
Mean Annual Change in May 1st SWE	-6.30 ± 6.95%	-5.9M m³ ± 6.5M m³
Total Loss	-5.85%	-94M m³

Figure 6: Watershed scale impacts of postfire effects and recovery in the Lower Granite Creek (LGC) subbasin during the ablation period (May 1st) for every year in the simulation. Postfire effects on snow albedo and forest structure caused net reductions in average May 1st SWE within the LGC subbasin in all but one year between 2000 and 2020, indicating that postfire effects on snow and forest structure cause lasting reductions in watershed-scale ablation season SWE for many years following fire. Further, the greatest losses in May 1st SWE did not occur immediately following each burn, but instead 3 to 5 years afterwards.

reduction of 5.85% in May 1st SWE over the 20-year modeling period, a total volume of >94M m^3 of additional snowmelt by May 1st (Figure 6).

3.5 Model Validation

Based on our validation of the modeled results using in-situ SWE measurements collected from within several of the burn regions, we overestimated SWE in both the base model (+40.22 ± 38.88%) and postfire snow albedo recovery model (+41.61 ± 46.29%) and both models were relatively close in accuracy (<1.5% difference). Both the base model and postfire snow albedo recovery model overestimated SWE in the individual fires and, again, showed similar levels of accuracy between one another (Table 4).

4 Discussion

Improved modeling of forest fires effects on snow albedo and forest structure incorporating postfire recovery allowed for volumetric watershed scale estimates of postfire reductions in

Table 4: Results of the model validation using field measurements of SWE collected from six of the burns between February and March of 2019. Percent error between the base/postfire albedo model were calculated against the field observations and the standard deviation was included when n > 1. Instances where the postfire snow albedo model performed better than the base model are in bold.

Fire	**Base Model**		**Postfire Snow Albedo Model**		**n**
	Avg. % Error (%)	SD (%)	Avg. % Error (%)	SD (%)	
Horsethief Canyon	+61.06	-	**+58.64**	-	1
Bull	+24.67	16.62	**+23.03**	**16.9**	16
Boulder	+40.71	11.02	+41.22	11.15	9
Cliff Creek	+40.4	13.47	+41.17	9.765	13
Lava Mountain	+48.89	12.04	**+46.18**	**15.13**	8
Roosevelt	+59.79	13.42	+67.89	11.96	13
Overall	+40.22	19.44	+41.61	23.15	60

snow-water storage and snow persistence. Peak snow-water storage decreased by ~4.5% and snow disappearance date advanced by over a week for at least 15 years following fire (Table 3). Sustained shifts in snow-water storage and snow-off date have the capacity to advance the timing of peak streamflow (Wieder et al., 2022), reduce spring and summertime soil moisture (Harpold, 2016; Westerling, 2016), extend growing seasons, and increase risk of future forest fire for many years beyond ignition (Abatzoglou & Kolden, 2013; Westerling, 2016). Our estimates discussed here highlight the importance of incorporating postfire effects on snow hydrology and can help to inform management of threatened water resources and forest fire mitigation in burned montane watersheds similar to our study region.

4.2. Immediate postfire effects on snow hydrology

Immediately following fire, postfire effects reduce snow-water storage by >8% and advance snow disappearance date by as much as 34 days (Table 3). These changes are primarily due to earlier melt onset from darkened postfire snow albedo (Figure A2; Figure 5) and become evident at or beyond the timing of peak snow-water storage (Figure 3c-d). Although increases in snow accumulation in March due to postfire forest structure degradation buffer later reductions in snow-water storage, these increases are ultimately overcome by profound reductions in snow-water storage between April and May (Figure 3d). Most of the reductions in snow-water storage due to postfire effects occur later in the snow season immediately following fire as insolation increases, temperatures warm, and postfire effects from darkened snow albedo become more pronounced (Figure 3c-d). Further, our estimates indicate that snowpack in burned forests disappears about one month earlier on average in the year immediately following fire (-34 days, sd = 7 days) and that this earlier disappearance is related to the advanced timing of snowmelt onset. Estimates of snow-water storage in burned montane forested watersheds made around the time of historical peak snow-water storage may not be adequate for accurate hydrological forecasting of snow-water reserves available later in the year as our estimates show the most profound postfire effects on snow-water storage occur later in the snow season.

4.3. Recovery of postfire effects on snow hydrology

Snow-water storage in burned forests largely shrank on average for the entire 15 year postfire recovery period (Table 3). Earlier melt onset advanced snow disappearance dates occurred in all modeled burns over all recovery periods (-31 to -8 days) and even post-recovery (16+ years

postfire: -5 days). Reductions in snow-water storage and earlier snow disappearance have been shown to drive decreases in minimum stream flows (Godsey et al., 2014; Hallema et al., 2018), lengthened growing seasons and the likelihood of spring and summertime water stress (Harpold, 2016; Westerling, 2016), and the occurrence, severity and extent of early season forest fire (Abatzoglou & Kolden, 2013; Westerling, 2016).

Although advances in snow disappearance dates and reductions in peak snow-water storage decreased on average over years since fire (Table 3), snowpack within burned forests showed widely varying responses in snow disappearance date timing (6 days $\leq$ sd(ΔSDD) $\leq$ 13 days) and peak snow-water storage reductions (8.71% $\leq$ sd(ΔSWE) $\leq$ 11.12%) over postfire recovery. These results highlight the difficulty in predicting the degree to which snow-water storage will be affected in burned watersheds over many years following fire, despite uniform parameterizations across each forest fire and a narrow scope of landscape and climate variability contained within the study region. Regions in the western United States rely on predictable spring runoff afforded by ample snow-water storage. Such variability in postfire snow hydrology responses within our relatively narrow scope of study compound with spatial and climactic variability across the western United States and increasing interannual variability in runoff timing due to the effects of climate change on snow-water storage and snowmelt timing (Li et al., 2017; Wieder et al., 2022).

Over the 15 years of postfire recovery, snow albedo and forest structure recovered from that of a recently burned forest towards an unburned open meadow as observed in Gersh et al (2022). Our parameterizations improved upon those of Gleason and Nolin (2016) by extending the parameterization of postfire snow hydrology immediately following fire to the recovery of snow albedo and forest structure over 15 years following fire. The results covered here provide evidence that snowpack in burned forests still exhibits reductions in peak snow-water storage (-0.30%, sd = 4.29%) and earlier snow disappearance date (-5 days, sd = 6 days) 16 years postfire and beyond (Table 3). Future parameterizations need to be extended to capture the full postfire recovery through regeneration to prefire conditions or other altered postfire states in order to calculate estimates of the complete effect of forest fire on snow hydrology.

4.4. Postfire effects on snow hydrology at the watershed scale

Watershed scale postfire effects reduced snow water storage and advanced snowmelt timing during the snowmelt period (May) across the 20 year modeling period (Figure 6). Postfire effects on snow albedo and forest structure from the Boulder, Bull and Cliff Creek fires caused annual reductions in May 1st snow volume within the Lower Granite Creek subbasin in all but one year (2011) of the 20-year modeling period (Figure 6). Trends in the recovery of postfire effects on May 1st SWE held at the watershed scale, with the greatest reductions in snow volume due to postfire effects occurring 3 to 5 years following each forest fire, rather than in the year immediately following each burn. Earlier snowmelt onset and peak snow-water storage caused by these forest fires led to earlier average annual snowmelt of 5.9M m^3 $\pm$ 6.5M m^3 per year and, over 20 years, resulted in a total of >94M m^3 of added early snowmelt than would occur in no-burn conditions. As a frame of reference, the USGS stream gauge at the outlet of the Lower Granite Creek sub-basin (USGS 13019438) measured an annual average streamflow volume of 29M m^3 per year between 1982 and 1993 (USGS, 2022). However, it is likely these calculations are underestimating the full extent of postfire effects on snow albedo and forest structure over

postfire recovery. Reductions in May 1st SWE were still visible as late as 2020 in the Boulder burn region, 4 years following the end of the postfire recovery period and postfire effects from the Bull (Ignition Date: 2010) and Cliff Creek fire (Ignition Date: 2016) were not captured over the extent of the full 15-year postfire recovery period (Figure 6).

As forest fires across the western United States become more frequent and extensive, how forest fire affects snow-water resources at the watershed scale and over many years following fire becomes an increasingly critical question. Multiple studies have demonstrated that reductions in peak snow volume can alter summer low flows (Godsey et al., 2014; Jenicek et al., 2018), especially in cold and dry continental snow zones (Hammond et al., 2018), and that annual river flow can be altered in watersheds burned for as little as 19% of their area (Hallema et al., 2018). The changes in peak snow-water storage due to postfire effects on snow hydrology modeled here have the capacity to alter resulting annual streamflow runoff (Godsey et al., 2014). Our findings provide the first three-dimensional, spatially-distributed, time varying, process-based estimates of postfire effects on snow hydrology and recovery over many years following fire and provide a basis for future estimates of associated effects on the timing and volume of spring streamflow.

4.5. Model validation

Both the base model and postfire albedo model overestimated SWE (+40.22%, sd = 19.44% vs. +41.61%, sd = 23.20%) in the individual fires and showed similar levels of accuracy between one another (Table 4). However, the field validation data for each burn were collected within close proximity to one another over the course of ~5 weeks in a single year while the modeled results span multiple decades and thousands of square kilometers, calculated in grids of 100 m^2. Although the model tended to overestimate SWE at the field validation sites, the model showed good agreement with 20 years of continuous data from SNOTEL sites spatially-distributed across the study region (Table 2) lending support for the estimates of postfire effects on snow over the broad spatial and time scales investigated in this study.

4.6. Uncertainties in modeling postfire effects on snow albedo and forest structure

We employed a postfire snow albedo and snow albedo decay parameterization developed in the Oregon Cascades to model postfire effects on snow hydrology in the Rocky Mountains introducing key uncertainties in how postfire effects on snow hydrology might differ between these two disparate snow climates and the associated influence on our results. However, research by Gleason & Nolin (2016) was the only published parameterization of postfire effects on snow albedo and snow albedo decay at the time of publication and thus it is uncertain how postfire effects on snow albedo might differ across these two snow climates. In addition, our parameterization of postfire forest structure modeled recovery in a simplified, linear fashion while previous work investigating postfire effects on forest structure in similar regions shows that delayed tree mortality can occur at an exponentially decaying rate following fire (Angers et al., 2011; Brown & DeByle, 1987) and can depend on many factors such as seed supply, distance to sources, and pre- and postfire climate (Stevens-Rumann & Morgan, 2019). The modeling capabilities of forest structure dynamics in the current iteration of SnowModel are limited, but

future expansions of SnowModel will allow for more precise estimates of postfire effects on forest structure and recovery and the resulting effects on snow hydrology.

5 Conclusions

Forest fire darkens snow albedo and degrades forest structure, increasing radiative forcing on snow for years following fire, and carrying with it the capacity to significantly alter snow evolution and, by extension, water supply over multi-decadal time scales. This study assessed the long-term water supply impacts of postfire effects on snow hydrology by incorporating an improved postfire snow albedo and forest structure recovery parameterization in a snow mass and energy balance model and estimating postfire effects on snow albedo and forest structure and recovery on peak SWE, SDD, and SWE volume reductions.

Immediately following forest fire, snowpack storage increased by up to 6.93% in early winter, but decreased by 8.43% during spring and up to 87.97% by May with earlier melt onset and 30+ day advanced snow disappearance. Following a 15 year postfire recovery period, burned forests still exhibited reduced peak snow-water storage of 0.30% and a 5 day earlier snow disappearance date due to the shift from forest to open meadow. Forest fires effects within the burned perimeter integrated over 15 years following fire amounted to an average 4.5% reduction on snow-water storage.

Watershed scale forest fire effects on snow-water storage and snowmelt are persistent for decades following fire. The results of this study show that forest fire has immediate, profound, and lasting effects on snow hydrology and water supply that last decades beyond the initial burn event and have hydrological implications beyond the forest fire perimeter. Quantification of changes in snow volume and snow melt on the snow-mass energy- balance using process-based snow models provide information critical to our understanding of the long-term impacts of an increasingly severe fire regime on the quantity and timing of freshwater originating from springtime snowmelt.

Acknowledgments

This research was funded by NASA as part of the Terrestrial Hydrology Program (Award #80NSSC19K0002). Special thanks to Glen Liston for his support in running SnowModel and troubleshooting our modifications and to Ryan Crumley for his support in initializing SnowModel.

Open Research

All data used to produce the results of this study including model inputs, model outputs, and SnowModel parametrization files are available through PDX Scholar at [Temporary link via Google Drive: https://drive.google.com/drive/folders/1exRuIPaU4sAqAHp3sJewWTch_WNMpe_T?usp=sharing].

References

Abatzoglou, J. T., & Kolden, C. A. (2013). Relationships between climate and macroscale area burned in the western United States. *International Journal of Wildland Fire*, *22*(7), 1003. https://doi.org/10.1071/WF13019

Angers, V. A., Gauthier, S., Drapeau, P., Jayen, K., & Bergeron, Y. (2011). Tree mortality and snag dynamics in North American boreal tree species after a wildfire: A long-term study. *International Journal of Wildland Fire*, *20*(6), 751. https://doi.org/10.1071/WF10010

Armitage, R. P., Alberto Ramirez, F., Mark Danson, F., & Ogunbadewa, E. Y. (2013). Probability of cloud-free observation conditions across Great Britain estimated using MODIS cloud mask. *Remote Sensing Letters*, *4*(5), 427–435. https://doi.org/10.1080/2150704X.2012.744486

Barnett, T. P., Adam, J. C., & Lettenmaier, D. P. (2005). Potential impacts of a warming climate on water availability in snow-dominated regions. *Nature*, *438*(7066), 303–309. https://doi.org/10.1038/nature04141

Brown, J. K., & DeByle, N. V. (1987). Fire damage, mortality, and suckering in aspen. *Canadian Journal of Forest Research*, *17*(9), 1100–1109. https://doi.org/10.1139/x87-168

Brown, O. L. I. (1951). The Clausius-Clapeyron equation. *Journal of Chemical Education*, *28*(8), 428. https://doi.org/10.1021/ed028p428

Buchhorn, M., Smets, B., Bertels, L., Roo, B. D., Lesiv, M., Tsendbazar, N.-E., Li, L., & Tarko, A. (2020). *Copernicus Global Land Service: Land Cover 100m: version 3 Globe 2015-2019: Product User Manual* (Dataset v3.0, doc issue 3.3). Zenodo. https://doi.org/10.5281/ZENODO.3938963

759 Campagnolo, M. L., Sun, Q., Liu, Y., Schaaf, C., Wang, Z., & Román, M. O. (2016). Estimating
760 the effective spatial resolution of the operational BRDF, albedo, and nadir reflectance
761 products from MODIS and VIIRS. *Remote Sensing of Environment*, *175*, 52–64.
762 https://doi.org/10.1016/j.rse.2015.12.033
763 Cescatti, A., Marcolla, B., Santhana Vannan, S. K., Pan, J. Y., Román, M. O., Yang, X., Ciais,
764 P., Cook, R. B., Law, B. E., Matteucci, G., Migliavacca, M., Moors, E., Richardson, A.
765 D., Seufert, G., & Schaaf, C. B. (2012). Intercomparison of MODIS albedo retrievals and
766 in situ measurements across the global FLUXNET network. *Remote Sensing of*
767 *Environment*, *121*, 323–334. https://doi.org/10.1016/j.rse.2012.02.019
768 Danielson, J. J., & Gesch, D. B. (2010). *Global Multi-resolution Terrain Elevation Data 2010*
769 *(GMTED2010)*.
770 Esri Inc. (2022). *2D, 3D & 4D GIS Mapping Software | ArcGIS Pro*. https://www.esri.com/en-
771 us/arcgis/products/arcgis-pro/overview
772 Finco, M., Quayle, B., Zhang, Y., Lecker, J., Megown, K. A., & Brewer, C. K. (2012).
773 Monitoring Trends and Burn Severity (MTBS): Monitoring wildfire activity for the past
774 quarter century using landsat data. *In: Morin, Randall S.; Liknes, Greg C., Comps.*
775 *Moving from Status to Trends: Forest Inventory and Analysis (FIA) Symposium 2012;*
776 *2012 December 4-6; Baltimore, MD. Gen. Tech. Rep. NRS-P-105. Newtown Square, PA:*
777 *U.S. Department of Agriculture, Forest Service, Northern Research Station. [CD-ROM]:*
778 *222-228.*, 222–228.
779 Gersh, M., Gleason, K. E., & Surunis, A. (2022). Forest Fire Effects on Landscape Snow Albedo
780 Recovery and Decay. *Remote Sensing*, *14*(16), 4079. https://doi.org/10.3390/rs14164079

781 Gleason, K. E., McConnell, J. R., Arienzo, M. M., Chellman, N., & Calvin, W. M. (2019). Four-
782 fold increase in solar forcing on snow in western U.S. burned forests since 1999. *Nature*
783 *Communications*, *10*(1), 2026. https://doi.org/10.1038/s41467-019-09935-y
784 Gleason, K. E., & Nolin, A. W. (2016). Charred forests accelerate snow albedo decay:
785 Parameterizing the post-fire radiative forcing on snow for three years following fire.
786 *Hydrological Processes*, *30*(21), 3855–3870. https://doi.org/10.1002/hyp.10897
787 Gleason, K. E., Nolin, A. W., & Roth, T. R. (2013). Charred forests increase snowmelt: Effects
788 of burned woody debris and incoming solar radiation on snow ablation: CHARRED
789 FORESTS INCREASE SNOWMELT. *Geophysical Research Letters*, *40*(17), 4654–
790 4661. https://doi.org/10.1002/grl.50896
791 Godsey, S. E., Kirchner, J. W., & Tague, C. L. (2014). Effects of changes in winter snowpacks
792 on summer low flows: Case studies in the Sierra Nevada, California, USA. *Hydrological*
793 *Processes*, *28*(19), 5048–5064. https://doi.org/10.1002/hyp.9943
794 Gorelick, N., Hancher, M., Dixon, M., Ilyushchenko, S., Thau, D., & Moore, R. (2017). Google
795 Earth Engine: Planetary-scale geospatial analysis for everyone. *Remote Sensing of*
796 *Environment*. https://doi.org/10.1016/j.rse.2017.06.031
797 Hale, K. E., Wlostowski, A. N., Badger, A. M., Musselman, K. N., Livneh, B., & Molotch, N. P.
798 (2022). Modeling streamflow sensitivity to climate warming and surface water inputs in a
799 montane catchment. *Journal of Hydrology: Regional Studies*, *39*, 100976.
800 https://doi.org/10.1016/j.ejrh.2021.100976
801 Hall, D. K., & Riggs, G. A. (2007). Accuracy assessment of the MODIS snow products.
802 *Hydrological Processes*, *21*(12), 1534–1547. https://doi.org/10.1002/hyp.6715

Hallema, D. W., Sun, G., Caldwell, P. V., Norman, S. P., Cohen, E. C., Liu, Y., Bladon, K. D., & McNulty, S. G. (2018). Burned forests impact water supplies. *Nature Communications*, *9*(1), 1307. https://doi.org/10.1038/s41467-018-03735-6

Hammond, J. C., Saavedra, F. A., & Kampf, S. K. (2018). How Does Snow Persistence Relate to Annual Streamflow in Mountain Watersheds of the Western U.S. With Wet Maritime and Dry Continental Climates? *Water Resources Research*, *54*(4), 2605–2623. https://doi.org/10.1002/2017WR021899

Harpold, A. A. (2016). Diverging sensitivity of soil water stress to changing snowmelt timing in the Western U.S. *Advances in Water Resources*, *92*, 116–129. https://doi.org/10.1016/j.advwatres.2016.03.017

Hiemstra, C. A., Liston, G. E., & Reiners, W. A. (2006). Observing, modelling, and validating snow redistribution by wind in a Wyoming upper treeline landscape. *Ecological Modelling*, *197*(1–2), 35–51. https://doi.org/10.1016/j.ecolmodel.2006.03.005

Jenicek, M., Seibert, J., & Staudinger, M. (2018). Modeling of Future Changes in Seasonal Snowpack and Impacts on Summer Low Flows in Alpine Catchments. *Water Resources Research*, *54*(1), 538–556. https://doi.org/10.1002/2017WR021648

Li, D., Wrzesien, M. L., Durand, M., Adam, J., & Lettenmaier, D. P. (2017). How much runoff originates as snow in the western United States, and how will that change in the future? *Geophysical Research Letters*, *44*(12), 6163–6172. https://doi.org/10.1002/2017GL073551

Liston, G. E., & Elder, K. (2006a). A Meteorological Distribution System for High-Resolution Terrestrial Modeling (MicroMet). *Journal of Hydrometeorology*, *7*(2), 217–234. https://doi.org/10.1175/JHM486.1

826 Liston, G. E., & Elder, K. (2006b). A Distributed Snow-Evolution Modeling System
827 (SnowModel). *Journal of Hydrometeorology*, *7*(6), 1259–1276.
828 https://doi.org/10.1175/JHM548.1
829 Liston, G. E., Haehnel, R. B., Sturm, M., Hiemstra, C. A., Berezovskaya, S., & Tabler, R. D.
830 (2007). Simulating complex snow distributions in windy environments using SnowTran-
831 3D. *Journal of Glaciology*, *53*(181), 241–256.
832 https://doi.org/10.3189/172756507782202865
833 Liston, G. E., & Hall, D. K. (1995). An energy-balance model of lake-ice evolution. *Journal of*
834 *Glaciology*, *41*(138), 373–382. https://doi.org/10.3189/S0022143000016245
835 Liston, G. E., Hiemstra, C. A., Elder, K., & Cline, D. W. (2008). Mesocell Study Area Snow
836 Distributions for the Cold Land Processes Experiment (CLPX). *Journal of*
837 *Hydrometeorology*, *9*(5), 957–976. https://doi.org/10.1175/2008JHM869.1
838 Luce, C. H., Abatzoglou, J. T., & Holden, Z. A. (2013). The Missing Mountain Water: Slower
839 Westerlies Decrease Orographic Enhancement in the Pacific Northwest USA. *Science*,
840 *342*(6164), 1360–1364. https://doi.org/10.1126/science.1242335
841 Lundquist, J. D., Dickerson-Lange, S. E., Lutz, J. A., & Cristea, N. C. (2013). Lower forest
842 density enhances snow retention in regions with warmer winters: A global framework
843 developed from plot-scale observations and modeling: Forests and Snow Retention.
844 *Water Resources Research*, *49*(10), 6356–6370. https://doi.org/10.1002/wrcr.20504
845 Mauricio Zambrano-Bigiarini. (2020). *HydroGOF: Goodness-of-fit functions for comparison of*
846 *simulated and observed hydrological time series* (0.4-0).
847 https://doi.org/10.5281/zenodo.839854

Moriasi, D. N., Arnold, J. G., Liew, M. W. V., Bingner, R. L., Harmel, R. D., & Veith, T. L. (2007). Model Evaluation Guidelines for Systematic Quantification of Accuracy in Watershed Simulations. *Transactions of the ASABE*, *50*(3), 885–900. https://doi.org/10.13031/2013.23153

Mote, P. W., Li, S., Lettenmaier, D. P., Xiao, M., & Engel, R. (2018). Dramatic declines in snowpack in the western US. *Npj Climate and Atmospheric Science*, *1*(1), 2. https://doi.org/10.1038/s41612-018-0012-1

Musselman, K. N., Molotch, N. P., & Brooks, P. D. (2008). Effects of vegetation on snow accumulation and ablation in a mid-latitude sub-alpine forest. *Hydrological Processes*, *22*(15), 2767–2776. https://doi.org/10.1002/hyp.7050

NOAA, C. (2021). *Climate Data Online (CDO)-The National Climatic Data Center's (NCDC) Climate Data Online (CDO) provides free access to NCDC's archive of historical weather and climate data in addition to station history information.| National Climatic Data Center (NCDC)*.

R Core Team. (2021). *R: A Language and Environment for Statistical Computing*. R Foundation for Statistical Computing. https://www.R-project.org/

Riggs, G. A., Hall, D. K., & Román, M. O. (2017). *Overview of NASA's MODIS and VIIRS Snow-Cover Earth SystemData Records* [Preprint]. Hydrology and Soil Science – Hydrology. https://doi.org/10.5194/essd-2017-25

Saha, S., Moorthi, S., Wu, X., Wang, J., Nadiga, S., Tripp, P., Behringer, D., Hou, Y.-T., Chuang, H., Iredell, M., Ek, M., Meng, J., Yang, R., Mendez, M. P., Dool, H. van den, Zhang, Q., Wang, W., Chen, M., & Becker, E. (2011). *NCEP Climate Forecast System Version 2 (CFSv2) 6-hourly Products*. Research Data Archive at the National Center for

Atmospheric Research, Computational and Information Systems Laboratory. https://doi.org/10.5065/D61C1TXF

Serreze, M. C., Clark, M. P., Armstrong, R. L., McGinnis, D. A., & Pulwarty, R. S. (1999). Characteristics of the western United States snowpack from snowpack telemetry (SNOTEL) data. *Water Resources Research*, *35*(7), 2145–2160. https://doi.org/10.1029/1999WR900090

Sexstone, G. A., Clow, D. W., Fassnacht, S. R., Liston, G. E., Hiemstra, C. A., Knowles, J. F., & Penn, C. A. (2018). Snow Sublimation in Mountain Environments and Its Sensitivity to Forest Disturbance and Climate Warming. *Water Resources Research*, *54*(2), 1191–1211. https://doi.org/10.1002/2017WR021172

Smoot, E. E., & Gleason, K. E. (2021). Forest Fires Reduce Snow-Water Storage and Advance the Timing of Snowmelt across the Western U.S. *Water*, *13*(24), Article 24. https://doi.org/10.3390/w13243533

SNOwpack TELemetry Network (SNOTEL) | Ag Data Commons. (2020). https://data.nal.usda.gov/dataset/snowpack-telemetry-network-snotel

Stevens, J. T. (2017). Scale-dependent effects of post-fire canopy cover on snowpack depth in montane coniferous forests. *Ecological Applications*, *27*(6), 1888–1900. https://doi.org/10.1002/eap.1575

Stevens-Rumann, C. S., & Morgan, P. (2019). Tree regeneration following wildfires in the western US: A review. *Fire Ecology*, *15*(1), 15. https://doi.org/10.1186/s42408-019-0032-1

Ueyama, M., Ichii, K., Iwata, H., Euskirchen, E. S., Zona, D., Rocha, A. V., Harazono, Y., Iwama, C., Nakai, T., & Oechel, W. C. (2014). Change in surface energy balance in

Alaska due to fire and spring warming, based on upscaling eddy covariance measurements: Change in high-latitude energy balance. *Journal of Geophysical Research: Biogeosciences*, *119*(10), 1947–1969. https://doi.org/10.1002/2014JG002717

U.S. Geological Survey National Geospatial Program. (2022). *USGS National Hydrography Dataset Plus High Resolution National Release 1 FileGDB* [Data set]. U.S. Geological Survey. https://doi.org/10.5066/P9WFOBQI

USGS Water Data for the Nation. (2022). https://waterdata.usgs.gov/nwis

Varhola, A., Coops, N. C., Weiler, M., & Moore, R. D. (2010). Forest canopy effects on snow accumulation and ablation: An integrative review of empirical results. *Journal of Hydrology*, *392*(3–4), 219–233. https://doi.org/10.1016/j.jhydrol.2010.08.009

Venables, W. N., & Ripley, B. D. (2002). *Modern Applied Statistics with S* (Fourth). Springer. https://www.stats.ox.ac.uk/pub/MASS4/

Westerling, A. L. (2016). Increasing western US forest wildfire activity: Sensitivity to changes in the timing of spring. *Philosophical Transactions of the Royal Society B: Biological Sciences*, *371*(1696), 20150178. https://doi.org/10.1098/rstb.2015.0178

Western Regional Climate Center. (2021). *RAWS USA Climate Archive*. https://raws.dri.edu/

Wieder, W. R., Kennedy, D., Lehner, F., Musselman, K. N., Rodgers, K. B., Rosenbloom, N., Simpson, I. R., & Yamaguchi, R. (2022). Pervasive alterations to snow-dominated ecosystem functions under climate change. *Proceedings of the National Academy of Sciences*, *119*(30), e2202393119. https://doi.org/10.1073/pnas.2202393119

Yuan, X., Wood, E. F., Luo, L., & Pan, M. (2011). A first look at Climate Forecast System version 2 (CFSv2) for hydrological seasonal prediction: A FIRST LOOK AT CFSv2. *Geophysical Research Letters*, *38*(13), n/a-n/a. https://doi.org/10.1029/2011GL047792

Appendix A: Snowpack Energy Balance and Significance Testing

Supporting plots and tables for postfire snowpack energy balance and supporting significance values for figures and tables included in the body of the text.

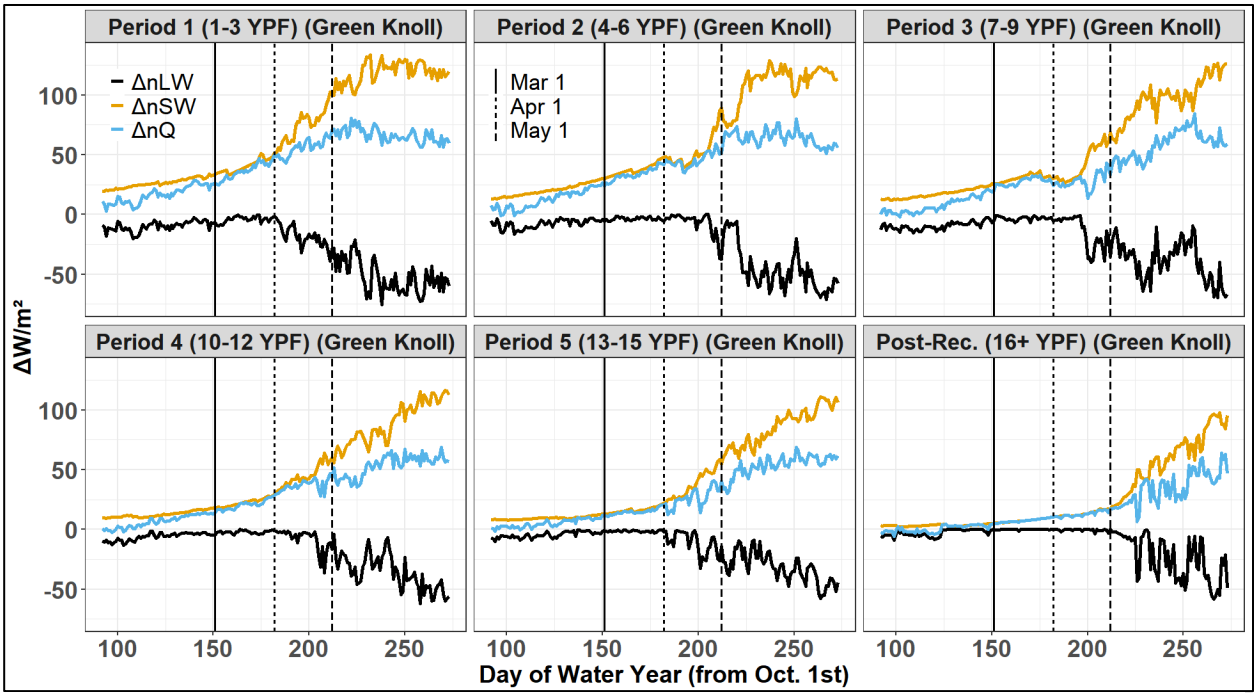

Figure A1: Difference between base model and postfire albedo model net components of the snowpack energy balance averaged over 3-year bins since burn for the Green Knoll forest fire only.

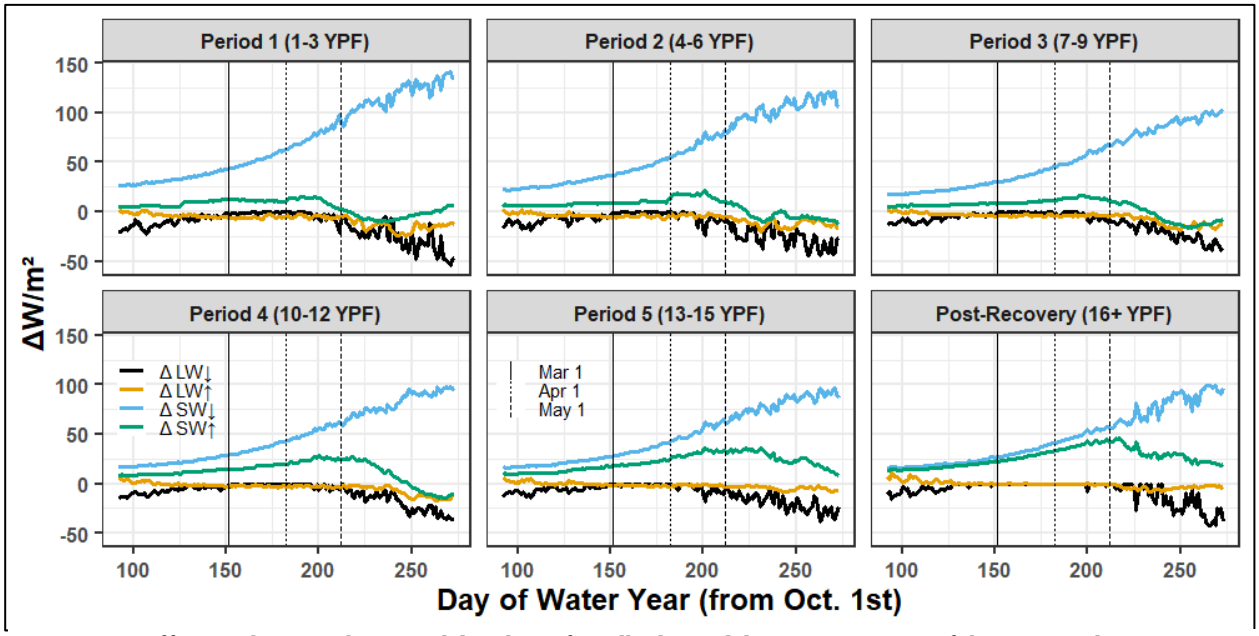

Figure A2: Difference between base model and postfire albedo model net components of the snowpack energy balance averaged over 3-year bins since burn over all modeled forest fires.

Table A1: Numerical results of significance testing performed on all modeled SWE results. For each result, 100 random pixels between the base model and postfire albedo model were selected and a two-sided Welch Two-Sample t-test was performed with an alpha value of 0.05.

Immediate Losses p-values	Welch Two-Sample t-test; two-sided; α = 0.05; n = 100							
	Boulder	Green Knoll	Purdy	Bull	Horsethief Canyon	Lava Mountain	Cliff Creek	Roosevelt
p-value	1.58E-04	0.0479	0.0016	0.438	1.12E-05	3.21E-18	1.99E-06	0.00261
Total Losses p-values	Welch Two-Sample t-test; two-sided; α = 0.05; n = 100							
	Boulder	Green Knoll	Purdy	Bull	Horsethief Canyon	Lava Mountain	Cliff Creek	Roosevelt
p-value	0.086	4.42E-04	0.420	0.0134	0.0045	1.71E-03	0.0041	0.0062
Period Averaged Peak SWE p-values	Welch Two-Sample t-test; two-sided; α = 0.05; n = 100							
	Boulder	Green Knoll	Purdy	Bull	Horsethief Canyon	Lava Mountain	Cliff Creek	Roosevelt
Period 1	1.35E-33	1.39E-33	0.00270	3.71E-04	6.22E-15	0.450	0.811	0.00559
Period 2	3.59E-07	8.04E-17	0.00436	5.23E-18	0.00367	0.00498	4.30E-05	
Period 3	0.00960	0.0023	3.22E-06	0.207	0.245			
Period 4	1.58E-22	0.0744	1.26E-14	0.834				
Period 5	0.414	0.00408	2.17E-08					
Post-Rec.	1.35E-08	4.74E-27						
March 1st SWE p-values	Welch Two-Sample t-test; two-sided; α = 0.05; n = 100							
	Boulder	Green Knoll	Purdy	Bull	Horsethief Canyon	Lava Mountain	Cliff Creek	Roosevelt
Period 1	4.84E-59	2.45E-34	2.82E-21	1.08E-25	1.23E-31	0.156	0.247	0.0176
Period 2	0.501	2.69E-24	1.29E-44	1.77E-18	1.66E-13	7.21E-47	1.61E-24	
Period 3	0.0406	4.80E-06	2.23E-27	0.213	9.84E-07			
Period 4	0.381	2.86E-13	0.0494	2.96E-25				
Period 5	0.00444	1.19E-05	6.21E-61					
Post-Rec.	4.94E-52	9.17E-44						
April 1st SWE p-values	Welch Two-Sample t-test; two-sided; α = 0.05; n = 100							
	Boulder	Green Knoll	Purdy	Bull	Horsethief Canyon	Lava Mountain	Cliff Creek	Roosevelt
Period 1	0.00152	2.77E-29	7.66E-09	2.90E-06	2.34E-17	3.20E-07	0.00245	0.144
Period 2	0.813	1.64E-20	0.00812	0.0328	0.0600	0.0159	0.0224	
Period 3	0.00679	0.574	0.101	2.36E-05	0.290			
Period 4	7.48E-19	9.67E-11	3.39E-23	0.0336				
Period 5	1.26E-05	0.109	3.01E-12					
Post-Rec.	1.13E-16	2.72E-08						
May 1st SWE p-values	Welch Two-Sample t-test; two-sided; α = 0.05; n = 100							
	Boulder	Green Knoll	Purdy	Bull	Horsethief Canyon	Lava Mountain	Cliff Creek	Roosevelt
Period 1	4.52E-101	4.07E-61	0.546	3.80E-05	5.39E-22	0.383	1.17E-07	4.27E-11
Period 2	1.63E-56	3.11E-30	0.0279	3.32E-27	2.42E-06	2.35E-12	3.01E-14	
Period 3	1.20E-19	0.232	0.199	0.0157	6.48E-08			
Period 4	1.09E-08	2.22E-04	5.82E-23	0.846				
Period 5	0.204	9.76E-18	0.00342					
Post-Rec.	1.58E-26	2.93E-06						

924 Table A2: Net shortwave radiative forcing *(*netSW*)* on snowpack averaged across all forest fires for the base model,
925 the postfire forest recovery model (Forest) and postfire snow albedo recovery model (Albedo) and the change in netSW attributable to postfire degradation of forest structure (ΔnSW_{forest}) or postfire effects on snow albedo (ΔnSW_{albedo}).

	Accumulation (net SW)						
	Base Model	**Forest Model**	**Albedo Model**	**Attribution (absolute)**		**Atribution (proportional)**	
Period	Mean (W/m²)	Mean (W/m²)	Mean (W/m²)	ΔnSW_{forest} (W/m²)	ΔnSW_{albedo} (W/m²)	ΔnSW_{forest} (%)	ΔnSW_{albedo} (%)
1	20.6 ± 2.76	43.2 ± 6.06	61.0 ± 9.16	22.6	17.8	52.3	29.2
2	24.1 ± 2.77	43.7 ± 5.49	59.1 ± 7.45	19.6	15.4	44.9	26.1
3	26.2 ± 2.79	41.5 ± 4.76	52.9 ± 6.17	15.3	11.4	36.9	21.6
4	23.8 ± 2.74	35.2 ± 4.31	41.8 ± 5.20	11.4	6.60	32.4	15.8
5	26.2 ± 3.53	35.8 ± 5.14	39.6 ± 5.87	9.60	3.80	26.8	9.60
Post-rec.	24.1 ± 2.79	29.7 ± 3.74	29.7 ± 3.74	5.60	0.00	18.9	0.00
	Ablation (net SW)						
	Base Model	**Forest Model**	**Albedo Model**	**Attribution (absolute)**		**Atribution (proportional)**	
Period	Mean (W/m²)	Mean (W/m²)	Mean (W/m²)	ΔnSW_{forest} (W/m²)	ΔnSW_{albedo} (W/m²)	ΔnSW_{forest} (%)	ΔnSW_{albedo} (%)
1	31.6 ± 5.05	68.7 ± 12.5	96.3 ± 17.3	37.1	27.6	54.0	28.7
2	33.4 ± 5.11	63.7 ± 10.6	85.1 ± 14.9	30.3	21.4	47.6	25.1
3	37.5 ± 4.80	61.3 ± 8.79	78.9 ± 11.7	23.8	17.6	38.8	22.3
4	34.1 ± 4.20	53.1 ± 7.33	62.6 ± 8.48	19.0	9.50	35.8	15.2
5	38.4 ± 5.92	54.6 ± 9.35	60.3 ± 10.3	16.2	5.70	29.7	9.45
Post-rec.	37.8 ± 5.11	48.0 ± 6.86	48.1 ± 6.92	10.2	0.10	21.3	0.21

Table A3: Net longwave radiative forcing on snowpack across all forest fires for both the base model (Base) and postfire snow albedo recovery model (Forest + Albedo) and the difference between the two models (Diff).

	Accumulation (net LW)					**Ablation (net LW)**				
	Base Model		**Forest + Albedo Model**			**Base Model**		**Forest + Albedo Model**		
Period	Mean (W/m²)	SD (W/m²)	Mean (W/m²)	SD (W/m²)	Diff (F&A - B) (W/m²)	Mean (W/m²)	SD (W/m²)	Mean (W/m²)	SD (W/m²)	Diff (F&A - B) (W/m²)
1	581	19.4	587.0	18.5	6.00	603	11.8	608	11.5	5.00
2	586	12	591	11.1	5.00	595	15.9	599	15	4.00
3	577	16.2	581	15.7	4.00	592	12.4	596	12	4.00
4	582	17.7	584	17.50	2.00	601	13.5	604	13.2	3.00
5	578	17.8	579	18.2	1.00	598	17.2	600	17.3	2.00
Post-rec.	606.0	15.4	606	15.3	0.00	624	12.1	624	12	0.00